remote sensing

MDPI

Article

Fine-Scale Identification and Functional Coupling Coordination of Production-Living-Ecological Space in Fuzhou's Rapid Urbanization Area, China

Chunyan Lu [1,2,*], Luyan Chen [1,2], Xinping Li [1], Zhihuang Huang [1] and Zhanyou Yan [1]

[1] College of Computer and Information Sciences, Fujian Agriculture and Forestry University, Fuzhou 350002, China; chenluyan@fafu.edu.cn (L.C.); lixinping@fafu.edu.cn (X.L.); huangzhihuang@fafu.edu.cn (Z.H.); yb_wxy@fafu.edu.cn (Z.Y.)
[2] Institute of Artificial Intelligence in Agriculture and Forestry, Fujian Agriculture and Forestry University, Fuzhou 350002, China
* Correspondence: luchunyan@fafu.edu.cn

Highlights

What are the main findings?

- The comprehensive PLES function of the study area increased markedly, and urban zones exhibit higher average comprehensive PLES function values than rural zones in the cell grid, indicating evident urban-rural functional heterogeneity.
- From 2012 to 2024, all PLES functional combinations experienced steady improvements in coupling coordination; socioeconomic factors serve as the dominant driving force to mitigate inter-functional conflicts and facilitate coordinated development.

What are the implications of the main findings?

- The integrated CCDM-GeoDetector framework based on multi-source geospatial data provides a replicable technical paradigm for evaluating territorial functional coordination in rapidly urbanized regions.
- The revealed urban-rural functional structure differentiation and coordinated evolution characteristics support differentiated zoning governance to balance urban construction, living demand, and ecological conservation.

Abstract

Accelerated urban expansion and socioeconomic growth have led to substantial changes in territorial spatial organization and growing pressures among spatial functions. Therefore, conducting fine-scale identification, functional evaluation, and coordination analysis of production-living-ecological space (PLES) carries practical value for improving spatial allocation and fostering harmonious regional coordination. By integrating remote sensing imagery and point-of-interest (POI) data, this study employed a hierarchical identification method combining the object-oriented random forest method with the DBSCAN (Density-Based Spatial Clustering of Applications with Noise) algorithm to map the PLES spatiotemporal evolution in Fuzhou's rapidly urbanizing territory over the 2012–2024 period. PLES functions were quantitatively assessed through a comprehensive evaluation index system, while the standard deviation ellipse, GeoDetector, and coupling coordination degree models were further employed to reveal their evolutionary patterns, driving mechanisms, and synergistic interactions. The results indicated that ecological-dominated spaces occupied the dominant share (nearly 63%). Meanwhile, living-dominated spaces expanded significantly, growing by 68.93 km^2 during the study period. The PLES comprehensive function increased by 15.50%, with the living function and production function

Check for updates

Academic Editor: Yuji Murayama

Received: 28 June 2026
Revised: 5 August 2026
Accepted: 6 August 2026
Published: 13 August 2026

Copyright: © 2026 by the authors. Licensee MDPI, Basel, Switzerland. This article is an open access article distributed under the terms and conditions of the Creative Commons Attribution (CC BY) license.

rising by 57.19% and 61.84%, respectively. Distinct spatial differentiation existed in PLES functions across urban and rural territories, shaping mutually complementary functional systems. The coupling coordination level of PLES functions continuously improved, although notable regional disparities existed, with highly coordinated areas concentrated in midwestern urban areas. PLES functional evolution was jointly driven by natural and socioeconomic factors, which interacted through nonlinear or two-factor enhancement effects. This study provides a replicable methodological framework for fine-scale PLES research and offers scientific support for regional spatial governance and high-quality coordinated development.

Keywords: production-living-ecological space (PLES); multi-source spatial data; function evaluation; coupling coordination; Fuzhou city

1. Introduction

Land, as the essential physical carrier of socioeconomic and ecological ecosystems, sustains socioeconomic development and ecological sustainability [1]. Differentiated spatial configuration and allocation enable territorial space to integrate production, living, and ecological functions, thereby facilitating socioeconomic development and supporting eco-environmental sustainability [2]. Accelerated economic development and urbanization have profoundly reshaped territorial space and land use patterns [3]. Globally, rapid urbanization and urban-rural restructuring have intensified conflicts among economic development, residential demands, and ecological protection, making the optimization of multifunctional land use a key issue in sustainable territorial governance [4]. Such rapid spatial restructuring has not only triggered a series of eco-environmental challenges, including pollution, excessive resource consumption, farmland loss, and ecosystem degradation, but also aggravated social inequalities manifested in uneven infrastructure provision, disparities in educational resources, housing shortages, and increasing traffic congestion [5,6]. Compared with traditional spatial zoning with rigid spatial boundaries defined by land attributes, the production-living-ecological space (PLES) emphasizes multifunctional coordination and synergistic governance. It provides a comprehensive and operable framework to improve land use efficiency, safeguard ecological security and enhance human well-being [7]. The formation and evolution of PLES stem from the interactive feedback between human socioeconomic activities and natural environmental constraints. Furthermore, disparities in resource allocation, industrial structure, and population agglomeration further trigger distinct urban-rural functional differentiation, generating asymmetric patterns of production supply, living services, and ecological security between urban and rural areas. Therefore, rational optimization of PLES spatial configuration and functional allocation has become an urgent need.

Accurate identification of PLES provides a scientific basis for regional coordinated planning and refined governance. Previous studies generally employed land use reclassification and comprehensive indicator-based evaluation methods to categorize PLES types. The land use reclassification method relies on remote sensing and geographic information system (GIS) technologies to reclassify each land use type into PLES types, either through direct assignment or scoring-based allocation [8]. In contrast, the comprehensive indicator-based evaluation method establishes an index system encompassing social, economic and natural determinants of PLES, and identifies PLES types via comprehensive assessment [9]. Although widely applied, these approaches are often limited by functional overlaps among PLES types and the low resolution of conventional data sources, thereby

restricting fine-scale PLES identification. Currently, the rapid development of GIS technologies has made point-of-interest (POI) data increasingly recognized as an important data resource for fine-scale PLES analysis. Characterized by massive data volume, easy acquisition and abundant geographic information, POI data are closely associated with diverse land multifunction [10]. POI data can intuitively reflect the actual land use types and spatial functional attributes, thereby providing robust support for the accurate identification and functional characterization of PLES [11]. Furthermore, pronounced disparities in natural conditions and socioeconomic development across urban and rural areas result in remarkable divergences in land utilization intensity and the spatial distribution of PLES. Regrettably, most existing studies adopt unified identification criteria across the entire region while ignoring the urban-rural functional differentiation and regional heterogeneity, resulting in systematic deviations in fine-scale characterization of territorial multifunctional patterns and restricting the accuracy of differentiated and refined PLES identification. Therefore, it is essential to establish methods for accurately identifying PLES types across different regions.

Quantitative evaluation of PLES functions can effectively reflect the development level and quality of regional space, and is widely recognized as an effective approach for mitigating conflicts in land utilization [12]. Existing studies typically quantify diverse PLES functions via established indicator systems [13]. However, most assessments remain confined to administrative unit scales, with coarse spatial resolution restricting refined spatial governance and targeted policy formulation. Given the intricate structures, pronounced spatial heterogeneity, and multi-scale characteristics of territorial space, evaluations conducted from an integrated regional perspective often overlook the urban-rural functional differentiation of PLES, thereby limiting a comprehensive understanding of the functional structure and spatial organization of territorial space. As urbanization has accelerated, the conflicts among production development, residential living demands, and ecological conservation have become increasingly prominent. Accordingly, it is hard to comprehensively depict the operation of regional spatial systems via a single functional perspective [14]. Therefore, scientifically evaluating the coordination among PLES functions has become an important approach for optimizing territorial spatial patterns and enhancing regional comprehensive benefits. To quantitatively characterize the coordinated development level of PLES functions, coupling coordination assessment has been widely adopted in regional and ecological research, which can effectively identify systemic coordination status and internal synergies among PLES subsystems, providing a scientific reference for targeted territorial spatial optimization and governance [15].

Fuzhou, an important central city on China's southeastern coast, requires a rational territorial spatial layout to underpin regional socioeconomic development, public welfare, and ecological security. Given the importance of PLES identification, functional evaluation, and coupling coordination analysis, this study focuses on the rapid urbanization area of Fuzhou City (RUAFC) and sets the following objectives: (1) employ a hierarchical classification method to realize fine-scale PLES identification and reveal spatiotemporal evolution patterns, (2) construct a comprehensive index system to quantify PLES functions and explore evolution driving mechanisms, (3) assess the coupling coordinated level of PLES functions, and (4) provide optimization strategies for the territorial spatial layout and coordinated evolution of PLES. To achieve these objectives, a unified analytical framework integrating fine-scale PLES identification, functional evaluation, and coupling coordination assessment was established. Multi-source datasets, including remote sensing images, POI data, geospatial environmental data, and socioeconomic statistics, were integrated into this framework. A hierarchical framework was established to achieve refined PLES identification, while the standard deviation ellipse (SDE) and GeoDetector model were

deployed to reveal the distribution pattern and driving factors of the spatiotemporal evolution of PLES comprehensive function. The coupling coordination degree model (CCDM) was adopted to quantify the coupling coordination of PLES functions. The proposed analytical framework provides a systematic approach for integrating refined PLES identification, functional evaluation, and coupling coordination assessment, while offering new insights into the functional organization and coordination characteristics of PLES, thereby supporting territorial spatial optimization and differentiated governance in rapidly urbanizing regions.

2. Materials and Methods

2.1. Study Area

The RUAFC encompasses six municipal districts of Fuzhou City, i.e., Gulou, Taijiang, Cangshan, Mawei, Jin'an, and Changle, which form the urban core of Fuzhou (Figure 1). Located within the longitude range of 119°10′E to 119°59′E and the latitude range of 25°40′N to 26°25′N, the study area covers 1676 km^2, occupying approximately 14.3% of Fuzhou's total administrative territory. This region's terrain is primarily composed of alluvial plains, low hills, and scattered mountains, with most elevations below 500 m.

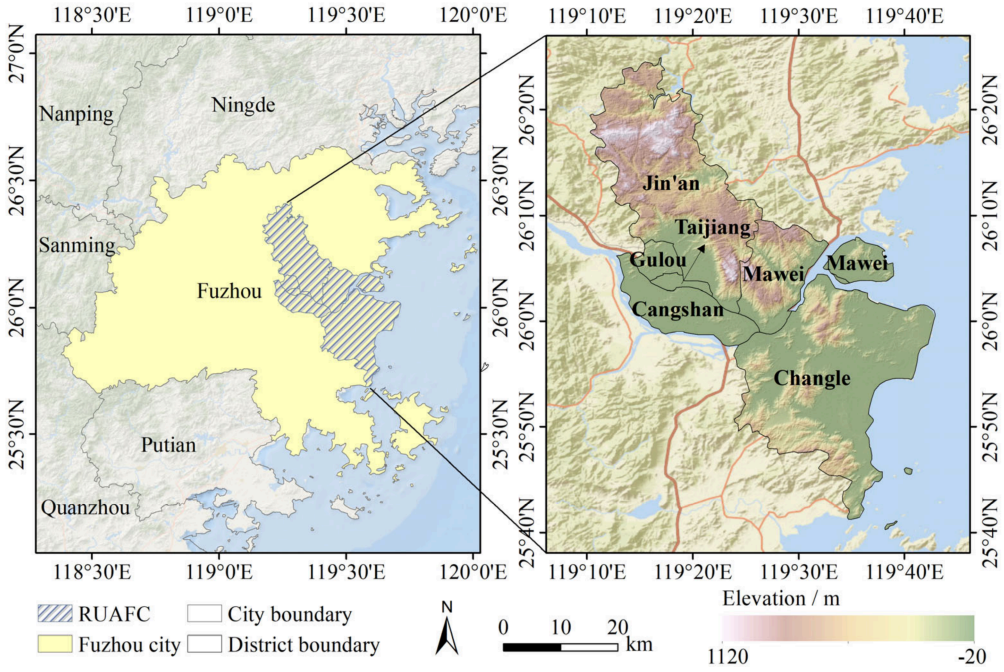


Figure 1. Location of the study area.

As Fuzhou's economic and cultural core, the RUAFC possesses a robust economy, sophisticated infrastructure, and dense population. In 2024, the aggregate GDP of the six districts reached 851.72 billion yuan, accounting for 59.83% of Fuzhou's total GDP. Nevertheless, rapid urban sprawl and population expansion have drastically reshaped the PLES spatial pattern within these districts, triggering several territorial spatial governance dilemmas, including urban functional conflicts and ecosystem degradation.

2.2. Data Sources and Pre-Processing

To identify the spatiotemporal distribution of PLES, the study integrated land use and POI data. For ensuring data quality and temporal consistency, the earliest available Landsat-8 OLI imagery closest to the 2012 baseline period was used to map land use for 2012, and Sentinel-2 MSI imagery was used for 2016, 2020, and 2024. To mitigate cloud interference,

images with cloud cover below 10% were first filtered on the Google Earth Engine (GEE) platform, followed by cloud masking to eliminate residual clouds and shadows, yielding high-quality imagery for subsequent analysis. Additionally, POI data serve as a reliable proxy of territorial spatial functions, as they reflect diverse urban geographic entities such as commercial facilities, educational institutions, healthcare services, and transportation facilities. This study collected POI data for 2012, 2016, 2020, and 2024 to assist in PLES identification. After standardized preprocessing, including duplicate removal, coordinate rectification, and invalid record filtering, irrelevant POI categories were excluded. 16 POI types were reclassified into corresponding PLES types according to their spatial functions.

To quantitatively evaluate PLES functions and detect driving factors, this study collected NPP/VIIRS nighttime light remote sensing data, 7 geospatial datasets (digital elevation model (DEM), POI, road network, population size, annual average precipitation, actual evapotranspiration, and bedrock depth), and 3 socioeconomic datasets (gross domestic product (GDP), primary industry output, and grain production). Slope and aspect were extracted via surface analysis using the DEM. Since socioeconomic statistics lack inherent spatial attributes, the study utilized the gridding approach proposed by Wang et al. [16] to spatially allocate socioeconomic indicators. Specifically, the secondary and tertiary industries output value was spatially gridded using NPP/VIIRS nighttime light imagery. Primary industry output and grain production were estimated via area-weighted calculations relying on corresponding land use type.

2.3. Land Use Classification Using Object-Oriented Random Forest Method

Considering the spatial layouts of regional land resources and research objectives, the study established a land use classification system (Table 1) and applied the object-oriented random forest method for land use classification. In contrast to pixel-based classification, object-oriented image analysis can effectively avoid salt-and-pepper effects and overcome intra-class spectral variations [17]. Meanwhile, the random forest algorithm delivers efficient and robust classification performance. A notable enhancement in land-use classification precision can be achieved by fusing the two approaches.

Table 1. Land use classification system and illustrative image.

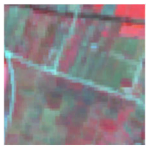
Land Use Type	Description	Image Features	Sample Image *
Built-up area	Anthropogenic impervious surfaces covered by built infrastructures, including industrial lands, residential built-up areas and traffic facilities	With gray, white, or bluish color, large continuous or aggregated patches, distinct boundaries, coarse texture	
Farmland	Cropland for agricultural production, consisting of paddy fields and dry cropland	With red, yellowish, or brown color, distinct boundaries, regular shape, homogeneous texture	
Woodland	Woody vegetation lands with canopy coverage exceeding 30%	With red or dark red color, irregular shape, uniform texture	

Table 1. *Cont.*

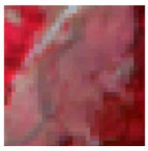
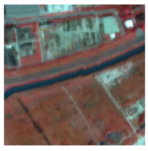
Land Use Type	Description	Image Features	Sample Image *
Grassland	Natural herbaceous vegetation with canopy coverage exceeding 30%	With light red or red color, indistinct boundary, fragmented patches, fine texture	
River	Linear natural water bodies with perennial continuous flow	With light blue, blue, or dark blue color, linear shape, fine texture	
Lake	Naturally formed stagnant water accumulation area	With light blue, blue, or dark blue, compact or irregular polygon shape, distinct boundaries, smooth texture	
Reservoir	Artificially enclosed and constructed large inland water bodies	With light blue, blue, or dark blue, large and irregular polygon shape, distinct boundaries, uniform texture	
Artificial pond	Artificially enclosed and constructed small inland water bodies	With blue or dark blue, small isolated patches, irregular or rounded shape, homogeneous texture	
Canal	Anthropogenic drainage and irrigation corridors	With light blue, blue, or dark blue, narrow straight or gently curved linear shape, regular width, smooth texture	
Aquaculture pond	Enclosed facilities for anthropogenic aquatic aquaculture	With light blue, blue, or dark blue color, regular shape, distinct boundaries, smooth texture	
Nearshore marine water	Coastal shallow marine water bodies adjacent to shorelines	With blue to dark blue, wide and continuous coastal distribution, gradual tonal transition, fine texture	
Mudflat	Intertidal muddy tidal flats	With dark gray or gray, flat and continuous patches, indistinct boundaries, uniform texture	

Table 1. *Cont.*

Land Use Type	Description	Image Features	Sample Image *
Floodplain	Fluvially deposited lowlands composed of sand, silt and pelite, located adjacent to river main channels and formed by periodic flood sedimentation	With a gray, light brown color, elongated or patchy shape along rivers, coarse texture	
Wetland	Waterlogged lands dominated by aquatic and helophytic vegetation, encompassing mangroves, salt marshes and herbaceous swamps	With light red or red, patchy or belt-like distribution, irregular shape, indistinct outline, and smooth texture	
Barren land	Areas with vegetation coverage less than 5%	With brown, yellowish, or gray, indistinct boundary, irregular shape, and uniform texture	

* The example images are the color composite image from Sentinel-2 MSI R:G:B = Band 8:Band 4: Band 3.

First, an object-oriented multi-resolution image segmentation algorithm was applied to the processed remote sensing image. Drawing on previous studies, the shape and compactness factors were set to 0.1 and 0.6, respectively [18]. This study adopted the segmentation scale optimization model developed by Lu et al. [19] to determine segmentation scale parameters. Second, image objects generated from optimal segmentation were used to extract 3 image feature categories, which include 4 spectral index types (Normalized Difference Vegetation Index, Enhanced Vegetation Index, Normalized Difference Built-up Index, Normalized Difference Water Index), band-specific statistical features (mean and standard deviation values of each spectral band), 6 texture feature types (Homogeneity, dissimilarity, entropy, correlation, contrast, and angular second moment), and 3 shape feature types (Compactness, convexity, and eccentricity). Subsequently, all extracted image features were imported into a random forest model for land use classification. This model exhibits high efficiency and robustness, achieving reliable classification results even with limited training samples [20]. Finally, the classification results were validated with reference sample points acquired via visual interpretation of Google Earth imagery. Classification results with overall accuracy above 90% were regarded as qualified; otherwise, the random forest classifier was iteratively trained until the classification precision met the threshold. The accuracy assessment results, including yearly confusion matrices, producer's accuracy, user's accuracy, F1 scores and Kappa coefficients, are shown in Tables S1 and S2 and Figure S1. The overall technical workflow is illustrated in Figure 2.

2.4. PLES Identification Based on the DBSCAN Algorithm

Accurate PLES identification is crucial for territorial spatial governance and sustainable development. Given significant disparities in spatial structure and functional characteristics between urban and rural areas, alongside blurred urban–rural boundaries driven by rapid urbanization, precise spatial delineation relying merely on a single threshold or administrative boundary proves challenging. Previous studies have confirmed that POI datasets can reflect human activity intensity efficiently, providing a reliable basis for distinguishing urban and rural areas [21]. Before clustering, multi-year Amap POI data were uniformly cleaned and classified to mitigate interannual discrepancies in coverage and completeness. The spatial patterns of POI density distribution were systematically examined, revealing

consistent spatial agglomeration characteristics across all years. Considering the uneven availability of rural POIs in earlier datasets, POI density was employed rather than raw POI counts to alleviate potential biases. The study employed a POI density-based spatial clustering method at a 3-ha hexagonal grid scale to delineate urban and rural zones, and further adopted a hierarchical identification framework to realize refined PLES identification.

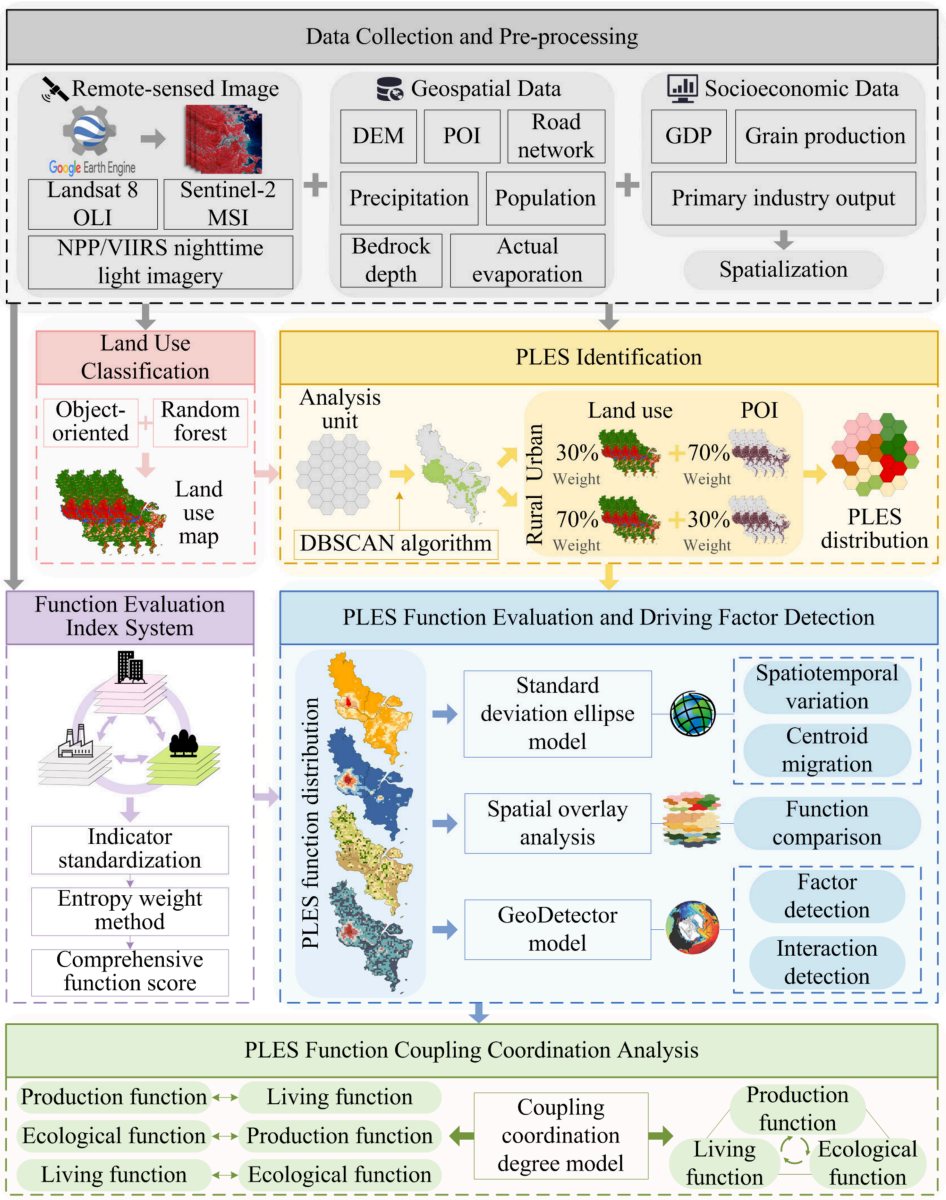


Figure 2. Overall technical flowchart of the study.

Based on previous studies [22,23], a 3-ha hexagonal grid covering the entire study area was generated. Taking each grid as the fundamental analysis unit, each PLES type's comprehensive score derived from land use data was calculated via weighted summation. Specifically, each weight was calculated by multiplying the correlation coefficients between land use and PLES types by their matching area proportion. The specific formula is shown as [24]:

$$S_{i,k}^{LU} = \sum_{j} (A_{i,j} \times M_{j,k}), \quad (1)$$

where $S_{i,k}^{LU}$ denotes the land use-based score of PLES type k in grid i, $A_{i,j}$ represents the area proportion of land use type j in grid i, and $M_{j,k}$ is the correlation coefficient between land use type j and PLES type k.

Subsequently, the density-based spatial clustering of applications with noise (DBSCAN) algorithm was deployed to conduct cluster analysis on POI data. Through comparative testing of diverse parameter-combination schemes, the neighborhood radius and minimum sample size were determined as 100 m and 10, respectively. High-density agglomeration areas were identified by setting the neighborhood radius and minimum sample number. Clustered points correspond to regions with intensive human activity aggregation, while noise points stand for areas with relatively weak anthropogenic activities [25]. Clustering outputs were spatially joined to hexagonal grid cells, and the share of clustered points inside each grid was computed. Based on comparative validation across multiple thresholds and reference datasets, a 50% clustered-point ratio was selected as the optimal threshold for urban-rural delineation. Grids with a clustered point ratio exceeding 50% were categorized as urban areas, whereas those with a ratio below 50% were classified as rural areas. Grids without any POI coverage were uniformly assigned to rural areas.

Furthermore, referring to the POI functional assignment framework proposed in prior research [26,27], the comprehensive score of each PLES type based on POI data was calculated as [28]:

$$S_{i,k}^{POI} = \sum_{m} (P_{i,m} \times W_{m,k}), \tag{2}$$

where $S_{i,k}^{POI}$ denotes the POI-based score of PLES type k in grid i, $P_{i,m}$ represents the proportion of POI type m in grid i, and $W_{m,k}$ is the correlation coefficient between POI type m and PLES type k.

The overall PLES comprehensive score was obtained by integrating land use-based and POI-based scores with different weights for urban and rural zones. The formula is defined as follows [29]:

$$S_{i,k} = \begin{cases} \alpha \cdot S_{i,k}^{LU} + (1-\alpha) \cdot S_{i,k}^{POI}, i \in urban \\ \beta \cdot S_{i,k}^{LU} + (1-\beta) \cdot S_{i,k}^{POI}, i \in rural \end{cases}, \tag{3}$$

where $S_{i,k}$ denotes the overall comprehensive score of PLES type k in grid i; α and β are weighting coefficients, designated as 0.3 and 0.7, respectively, to balance the contributions of land use and POI data, with different weights applied to urban and rural areas.

Finally, the scores of each grid were summarized by space type, and the PLES type of each grid was determined according to the proportion of scores for each type. The proportion of each PLES type was calculated as [8]:

$$R_{i,k} = \frac{S_{i.k}}{\sum_{k=1}^{n} S_{i,k}}, \tag{4}$$

where $R_{i,k}$ represents the proportion of space type k in grid i. Considering the fragmented landscape pattern and high spatial heterogeneity across this mountainous study area, a 70% threshold was adopted to ensure that the identified PLES type reflects the dominant spatial function. Accordingly, a grid cell was classified as a single space when the proportion of one space type was greater than or equal to 70%; otherwise, the two spaces with the highest proportions were identified to define the mixed space. In the study, the PLES at the 3-ha hexagonal grid scale was delineated into 9 types, including 3 single space types and 6 mixed space types.

2.5. Indicator-Based Evaluation of PLES Functions

Clarifying territorial spatial functions facilitates the formulation of targeted land use policies and effective spatial zoning management [30]. To quantitatively assess PLES functions, this study constructed a function evaluation indicator system based on the connotation of PLES and previous relevant studies. The system comprised 3 primary functional dimensions, 6 sub-functions, and 12 indicators in total, with detailed descriptions of all indicators presented in Figure 3. After normalizing all indicators, the entropy weight approach was utilized to compute scores for each sub-function type and the integrated comprehensive function. Finally, the delineated PLES type and the calculated function value were spatially overlaid to conduct statistical analysis on the functional characteristics of each PLES type.

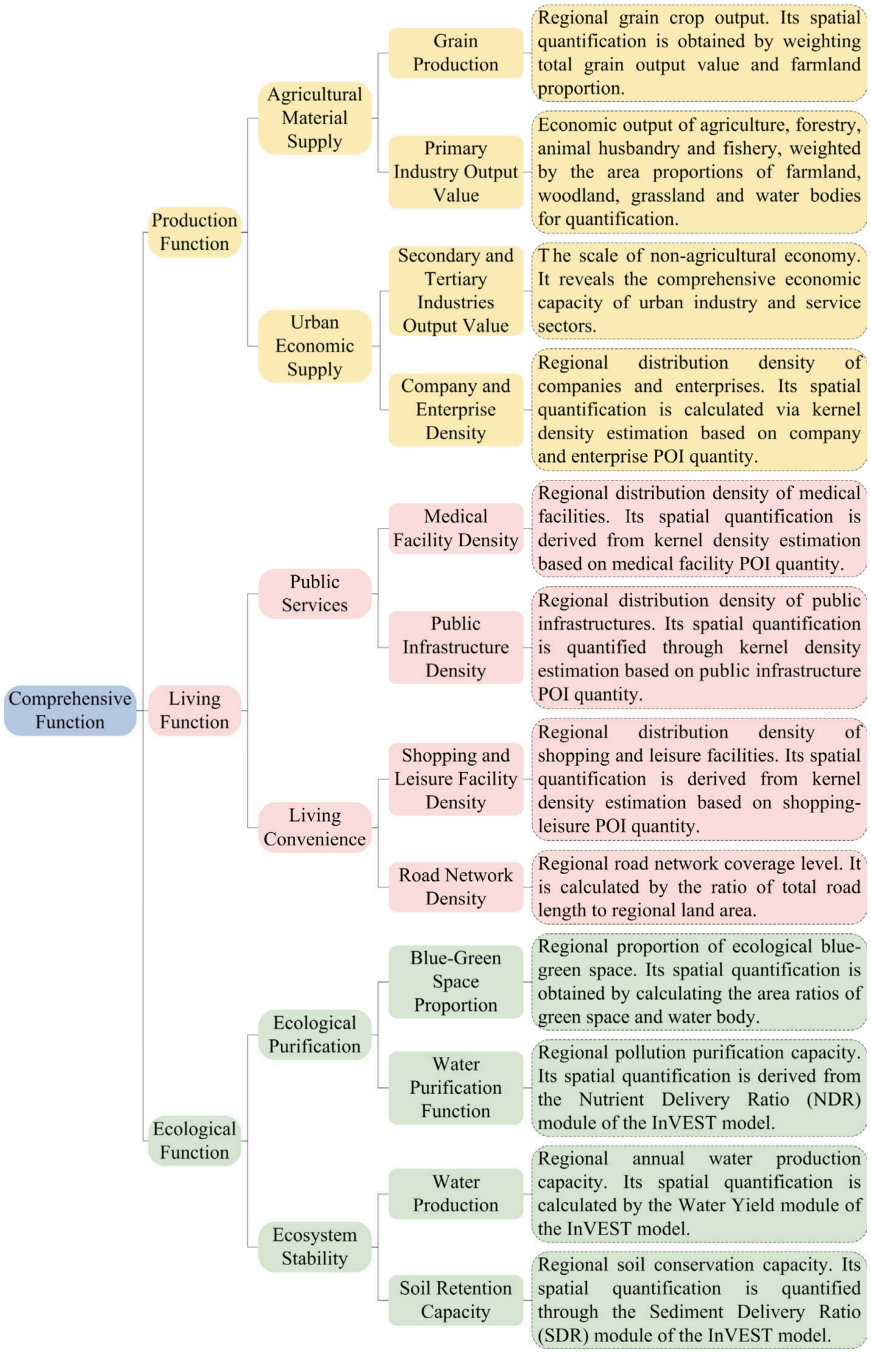


Figure 3. Function evaluation index system of the PLES.

2.6. PLES Spatiotemporal Evolution Analysis

To quantify the spatiotemporal dynamics of the PLES comprehensive function, the SDE model was adopted, which thoroughly characterizes the spatial distribution and directional dynamics of the functional space through the ellipse area, long/short axis, centroid, and azimuth. The formulas are as follow [31]:

$$(\overline{U}_w, \overline{V}_w) = \left(\frac{\sum_{i=1}^{n} w_i u_i}{\sum_{i=1}^{n} w_i}, \frac{\sum_{i=1}^{n} w_i v_i}{\sum_{i=1}^{n} w_i} \right), \tag{5}$$

$$\tan\theta = \frac{\left(\sum_{i=1}^{n} w_i \overline{u}_i^2 - \sum_{i=1}^{n} w_i \overline{v}_i^2 \right) + \sqrt{\left(\sum_{i=1}^{n} w_i \overline{u}_i^2 - \sum_{i=1}^{n} w_i \overline{v}_i^2 \right)^2 + 4 \sum_{i=1}^{n} (w_i \overline{u}_i \overline{v}_i)^2}}{2 \sum_{i=1}^{n} w_i^2 \overline{u}_i \overline{v}_i}, \tag{6}$$

$$\sigma_u = \sqrt{\frac{\sum_{i=1}^{n} (\overline{u}_i - \overline{U})^2}{n}}, \sigma_v = \sqrt{\frac{\sum_{i=1}^{n} (\overline{v}_i - \overline{V})^2}{n}}, \tag{7}$$

where $(\overline{U}_w, \overline{V}_w)$ denotes SDE centroid coordinates. w_i refers to the weight assigned to the i-th district. u_i and v_i stand for the longitude and latitude coordinates of the i-th district, respectively. θ represents the clockwise azimuth formed by the SDE major axis and the due north axis. $\overline{u}_i$ and $\overline{v}_i$ denote the coordinate offsets from the i-th district to the SDE centroid, correspondingly. σ_u indicates the SDE long axis, σ_v indicates the short axis. $\overline{U}$ and $\overline{V}$ are the mean centers of the longitude and latitude coordinates across all districts, respectively.

2.7. Coupling Coordination Analysis of PLES Functions

The CCDM serves to assess the coordinated development level among multiple systems [32]. Given the significant interactions among PLES functions in the process of socioeconomic development, the study adopts the CCDM to measure their coupling coordination. The calculation formulas for the CCDM are as follows [33]:

$$C = 3 \times \left[\frac{S \times L \times N}{(S + L + N)^3} \right]^{1/3}, \tag{8}$$

$$T = \omega S + \eta L + \kappa N, \tag{9}$$

$$D = \sqrt{C \times T}, \tag{10}$$

$$C_1 = 2 \times \left[\frac{S \times L}{(S + L)^2} \right]^{1/2}, C_2 = 2 \times \left[\frac{S \times N}{(S + N)^2} \right]^{1/2}, C_3 = 2 \times \left[\frac{L \times N}{(L + N)^2} \right]^{1/2}, \tag{11}$$

$$T_1 = \omega S + \eta L,\ T_2 = \omega S + \kappa N,\ T_3 = \eta L + \kappa N, \tag{12}$$

$$D_i = \sqrt{C_i \times T_i},\ i = 1, 2, 3, \tag{13}$$

where C denotes the PLES function coupling degree. C_1, C_2 and C_3 are the coupling degrees of production-living, production-ecological, and living-ecological functions, respectively. T is the coordination index. T_1, T_2, T_3 correspond to the coordination indices of the three pairwise functional combinations. S, L and N are the functional values of the production, living, and ecological functions, respectively. D represents the PLES function coupling coordination degree. D_i refers to the coupling coordination degree of the i-th pairwise functional subsystem. ω, η, and κ denote the undetermined coefficients for the production,

living, and ecological functions, respectively. Considering the equivalent contributions of the three functions to urban evolution, the coefficients are set as $\omega = \eta = \kappa = 1/3$ [34]. When calculating pairwise functional coordination, the two involved functions share equal weight, thus $\omega = \eta = \kappa = 1/2$ [35].

Combining the classification standard proposed by Jiang et al. [36] and the context of this study, the coupling coordination degrees of PLES functions are divided into five levels (Table 2).

Table 2. Types of coupling coordination degree of PLES functions.

Coupling Degree	Level	Coupling Coordination Degree	Level
[0, 0.20]	Low-level coupling	[0, 0.25]	Severe imbalance
(0.20, 0.40]	Antagonistic coupling	(0.25, 0.40]	Moderate imbalance
(0.40, 0.60]	Adaptive coupling	(0.40, 0.55]	Basic coordination
(0.60, 0.80]	High-level coupling	(0.55, 0.70]	Moderate coordination
(0.80, 1.00]	Benign resonant coupling	(0.70, 1.00]	High-level coordination

2.8. Detection of Influencing Factors for PLES Functions

To reveal the processes that underlie PLES functions' spatial heterogeneity, the GeoDetector model was applied to reveal spatial differentiation and identify the dominant driving factors. All continuous driving variables were discretized into five strata using the natural breaks (Jenks) classification method prior to GeoDetector analysis. Unlike conventional statistical methods, the GeoDetector can assess both the independent explanatory capacity of single factors and the interaction effects between paired factors [37]. Accordingly, factor and interaction detections were performed to explore the individual and synergistic influences of driving factors on PLES functions. The q-statistic was used to quantify each factor's explanatory power, which is expressed as follows [38]:

$$q = 1 - \frac{\sum_{i=1}^{L} N_i \sigma_i^2}{N\sigma^2}, \tag{14}$$

where i refers to the stratum of the dependent variable. N_i and N are the sample quantities of each stratum and the total study area, respectively. σ_i^2 and σ^2 denote the variances of each stratum and the total study area, respectively. The statistic q ranges from 0 to 1, with higher values signifying stronger explanatory capacity.

By comparing the joint interpretative contribution of paired drivers with the explanatory strength of each single factor, interaction detection can identify whether their composite influences on response indicators are mutually enhanced, weakened, or independent [39]. Table 3 presents the different interaction types and their corresponding interpretations for the joint influence of paired variables. Considering the natural and socioeconomic conditions, seven driving factors were incorporated into the analysis, i.e., elevation, slope, population density, nighttime light intensity, GDP, aspect, and distance to water bodies.

Table 3. Interaction types of dual driving factors.

Judgment Criteria	Interaction Type
$q(x_1 \cap x_2) = q(x_1) + q(x_2)$	Mutual independence
$q(x_1 \cap x_2) > q(x_1) + q(x_2)$	Nonlinear enhancement
$q(x_1 \cap x_2) < \mathrm{Min}(q(x_1), q(x_2))$	Nonlinear attenuation
$q(x_1 \cap x_2) > \mathrm{Max}(q(x_1), q(x_2))$	Two-factor interaction enhancement

Table 3. *Cont.*

Judgment Criteria	Interaction Type
$\mathrm{Min}(q(x_1), q(x_2)) < q(x_1 \cap x_2) < \mathrm{Max}(q(x_1), q(x_2))$	Single-factor nonlinear attenuation

Note: $q(x_1 \cap x_2)$ measures the extent to which the interaction of x_1 and x_2 influences the dependent variable. $q(x_1)$ and $q(x_2)$ denote the individual effects of x_1 and x_2, respectively. Min($q(x_1)$, q(x_2)) and Max($q(x_1)$, $q(x_2)$) are the minimum and maximum of $q(x_1)$ and $q(x_2)$, respectively.

3. Results

3.1. Spatiotemporal Dynamics of PLES

Based on the PLES hierarchical identification, the spatiotemporal layout of PLES was obtained from 2012 to 2024 (Figure 4). Ecologically dominated single and mixed space types (i.e., ecological space, ecological-production space and ecological-living space) prevailed through all years, covering approximately 63% and were primarily concentrated in northwestern rural areas (i.e., Jin'an and Mawei). Living-dominated space types (i.e., living space, living-production space and living-ecological space) were largely distributed in midwestern urban areas (i.e., Gulou, Taijiang, Cangshan, and the southern part of Jin'an), occupying over 18% of the study region. Production-dominated space types (i.e., production space, production-living space and production-ecological space) clustered in southeast urban-rural integrated areas (i.e., Changle and the eastern part of Mawei), covering approximately 17% of the total territory.

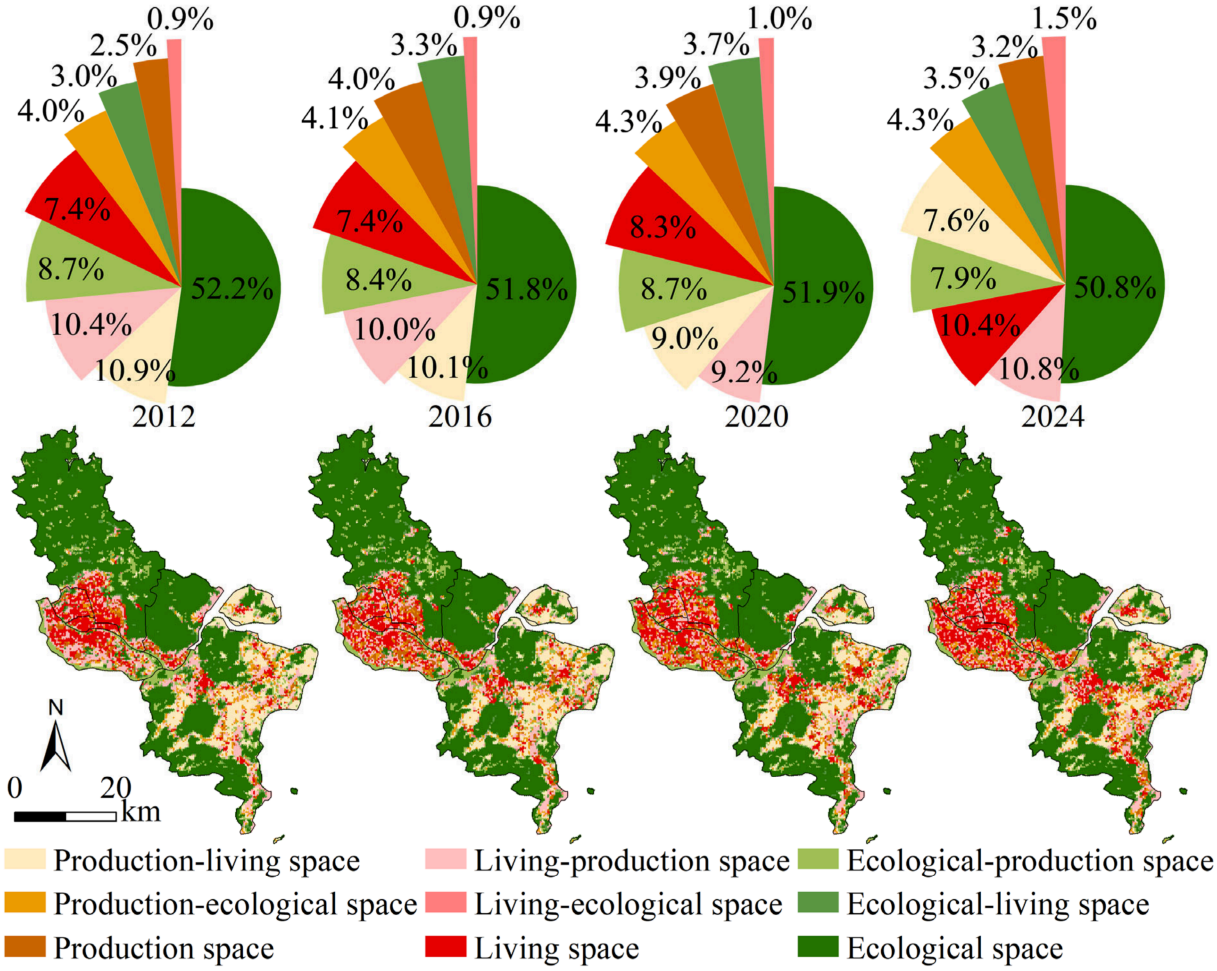


Figure 4. The spatiotemporal distribution of PLES in the study area from 2012 to 2024.

During the study period, living space experienced the most prominent expansion, with a total area growth of 53.09 km^2. Ecological-living, living-ecological, living-production, production-ecological, and production spaces also expanded at different magnitudes, rising by 7.19 km^2, 10.34 km^2, 5.50 km^2, 5.24 km^2, and 12.92 km^2, respectively. By contrast, production-living space decreased sharply, with an annual reduction of 4.74 km^2. Ecological-production space and ecological space also suffered varying degrees of shrinkage, with total area losses of 14.26 km^2 and 23.95 km^2 from 2012 to 2024.

The conversion of PLES types in the RUAFC was quantified via spatial overlay analysis (Figure 5). The magnitude of PLES transitions intensified continuously over time, and the total converted area reached 207.14 km^2, 346.08 km^2 and 358.44 km^2 for the three successive periods, respectively. The transformed areas were primarily concentrated in midwestern urban areas (i.e., Gulou, Taijiang, Cangshan, and southern Jin'an), where transitions between living- and production-dominated spaces were the most pronounced. Specifically, living-dominated space experienced the greatest expansion, increasing by 68.93 km^2, mainly derived from conversions of production, production-ecological, and production-living spaces. Conversely, production-dominated space exhibited the most substantial shrinkage, with a total area reduction of 37.91 km^2, and was primarily transformed into living-production and living spaces. Ecologically dominated space also declined by 31.02 km^2, largely converted to living, living-production, and production spaces.

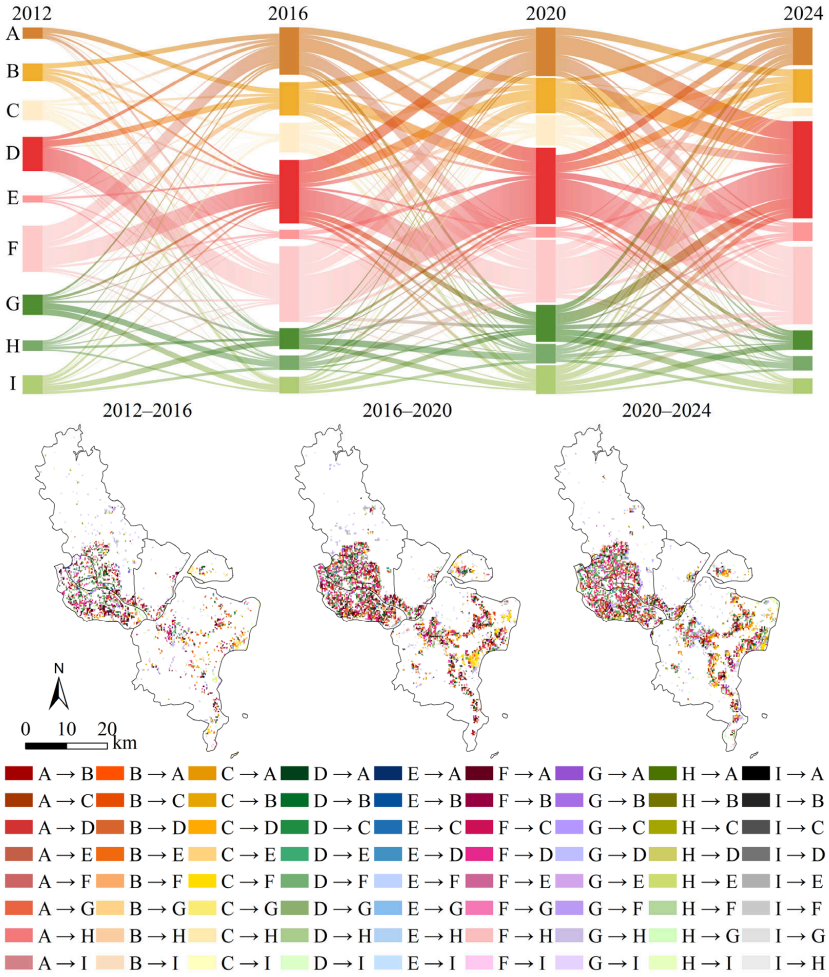


Figure 5. The spatiotemporal distribution of different PLES conversions during 2012–2024 in the study area (A is production space, B is production-ecological space, C is production-living space, D is living space, E is living-ecological space, F is living-production space, G is ecological space, H is ecological-living space, I is ecological-production space).

3.2. Spatiotemporal Evolution of PLES Function

Derived from the PLES functions evaluation indicator system, the assessment results of sub-functions and comprehensive functions from 2012 to 2024 were obtained (Figure 6). During the study period, high-value areas of production, living, and comprehensive functions were clustered in the core urban area (i.e., Gulou and Jin'an) and experienced continuous outward expansion. By comparison, ecological functions exhibited a completely reversed trend, with high-value areas aggregated in rural zones of Taijiang, Mawei, and western Changle, and maintaining relatively stable throughout the study period.

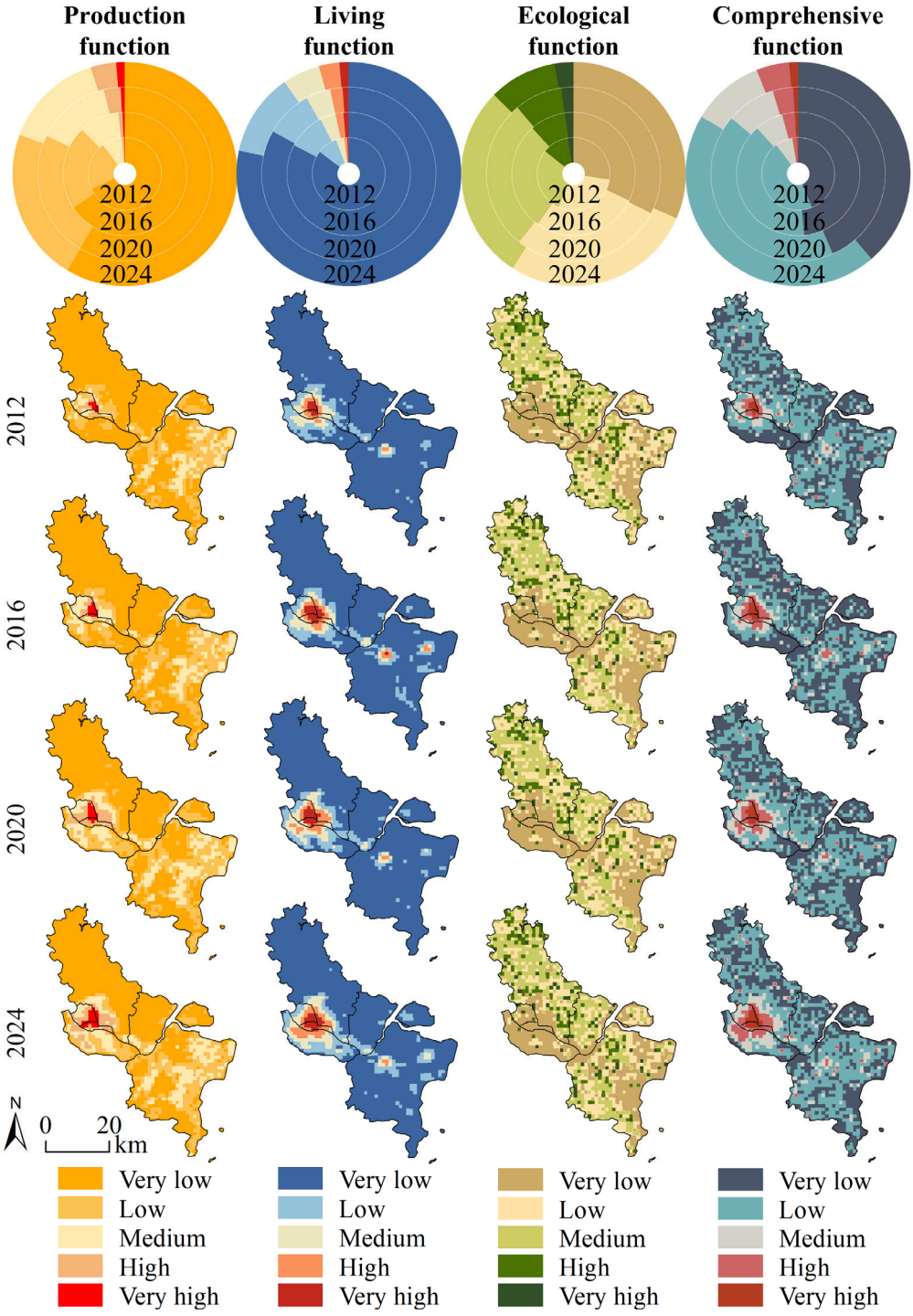


Figure 6. The spatiotemporal distribution of PLES functions in the study area from 2012 to 2024.

Based on the SDE model analysis, the spatiotemporal dynamics of the comprehensive function of PLES were characterized (Figure 7). The centroid of the PLES comprehensive function migrated from the southeast to the southwest over 2012–2024, indicating a southwestward shift in the center of the spatial distribution of comprehensive functions. Meanwhile, the SDE azimuth changed only slightly, from 142.64° in 2012 to 141.17° in 2024. The overall orientation of the spatial distribution remained relatively stable throughout the study period. This finding indicates that the primary development axis of PLES comprehensive functions underwent a slight overall southeastward adjustment.

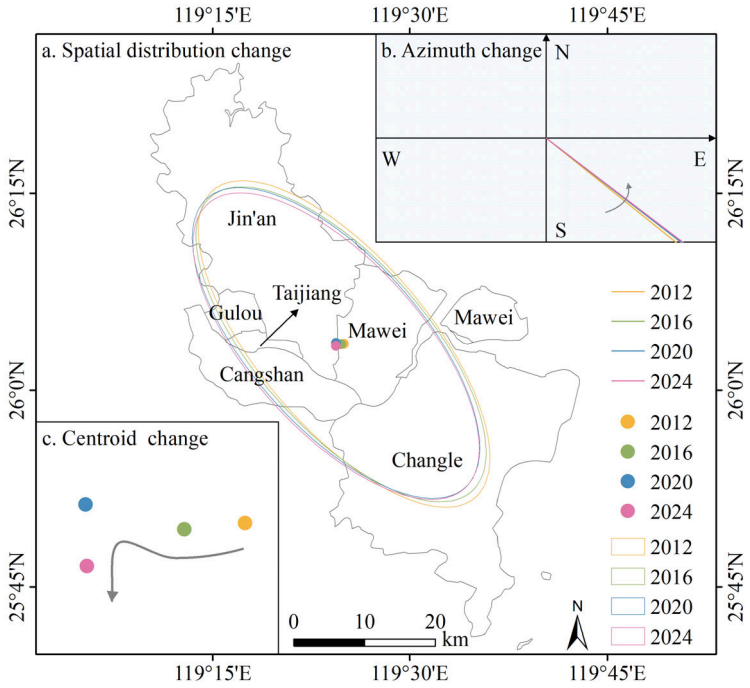


Figure 7. Spatiotemporal evolution characteristics of PLES comprehensive function in the study area from 2012 to 2024. (**a**) Spatial distribution of SDE from 2012 to 2024; (**b**) azimuth change of SDE from 2012 to 2024; (**c**) centroid migration route of SDE from 2012 to 2024.

3.3. Comprehensive Function Differences in Urban and Rural PLES Types

The comprehensive functional values of each PLES type in urban and rural areas of the study area from 2012 to 2024 and their corresponding average values at the grid scale were obtained by spatial overlay analysis and category aggregation (Table 4 and Figure 8). The share of comprehensive function contributed by ecological space declined from 48.28% in 2012 to 40.68% in 2024, with an overall change rate of −2.68%. Similarly, the proportions of the comprehensive functions of ecological-production and production-living spaces also exhibited a declining tendency, decreasing by 1.03% and 3.63%, respectively. Among these, the comprehensive function of living-ecological space witnessed the most striking growth, featuring a variation rate of 136.38%. For production- and living-related PLES categories, i.e., living, living-production, ecological-living, production, and production-ecological spaces, their comprehensive function change rates reached 81.12%, 48.97%, 22.01%, 32.83%, and 21.78%, respectively.

Differentiated functional structures existed between urban and rural zones in RUAFC. At the single grid unit scale, the average comprehensive functional score of each space type in urban zones was generally higher than that in rural zones. From an overall regional perspective, the comprehensive function values of ecological-dominated spaces were prominent in rural areas, whereas those of living-dominated spaces were more prominent in urban areas, forming a complementary and symbiotic urban-rural functional system.

Table 4. Average value of comprehensive function of each PLES type at grid scale from 2012 to 2024.

PLES Type	2012		2016		2020		2024	
	Urban	Rural	Urban	Rural	Urban	Rural	Urban	Rural
Ecological space	0.49	0.41	0.48	0.39	0.50	0.40	0.56	0.41
Ecological-living space	0.43	0.38	0.47	0.36	0.56	0.38	0.61	0.39
Ecological-production space	0.33	0.00	0.33	0.35	0.37	0.36	0.44	0.38
Living space	0.78	0.37	0.90	0.00	0.91	0.36	1.00	0.39
Living-ecological space	0.56	0.36	0.62	0.33	0.67	0.35	0.88	0.37
Living-production space	0.50	0.33	0.71	0.34	0.88	0.35	0.89	0.35
Production space	0.53	0.45	0.50	0.00	0.54	0.00	0.54	0.58
Production-ecological space	0.64	0.40	0.79	0.40	0.83	0.42	0.72	0.45
Production-living space	0.45	0.42	0.48	0.40	0.48	0.41	0.53	0.45

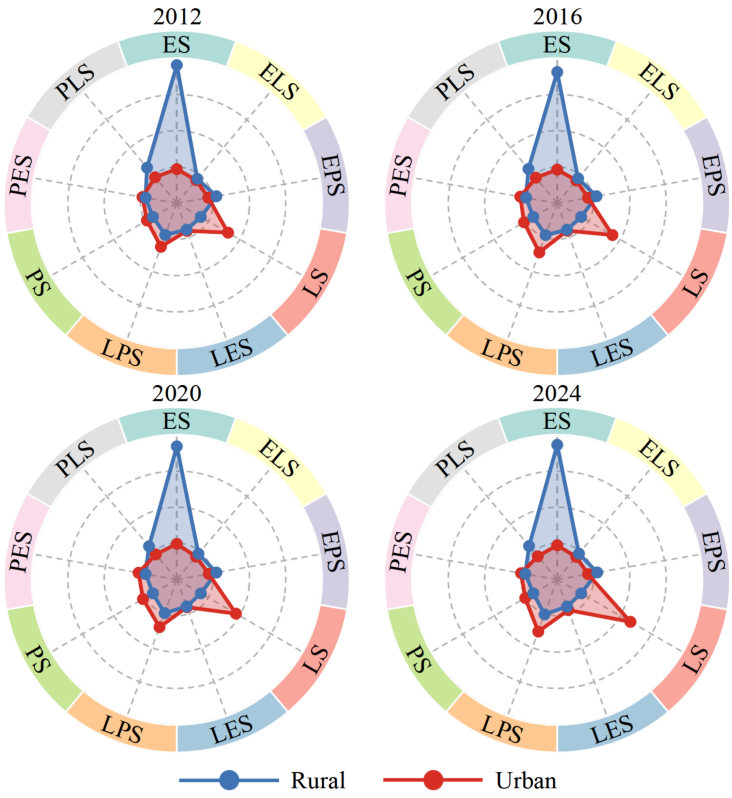


Figure 8. Comprehensive function values of different PLES types in urban and rural zones of the study area during 2012–2024. (PS is production space, PES is production-ecological space, PLS is production-living space, LS is living space, LES is living-ecological space, LPS is living-production space, ES is ecological space, ELS is ecological-living space, EPS is ecological-production space).

3.4. Spatiotemporal Evolution of Coupling Coordination Among PLES Functions

Based on the CCDM, the spatial distribution of coupling coordination among PLES functions was obtained from 2012 to 2024 (Figure 9). In terms of the coupling degrees between diverse functional combinations, although certain fluctuations occurred during 2012–2024, the proportions of low-level, adaptive and high-level couplings all displayed declining trends for four functional systems (i.e., production-ecological, production-living, living-ecological, and production-living-ecological). By contrast, their benign resonant coupling levels sustained steady growth, with respective increases of 27.20%, 6.33%, 11.33% and 15.38%. Notably, for antagonistic coupling levels, all other functional systems displayed rising trends, while only production-living coupling presented a declining tendency. Regarding the coupling coordination degree between different functional combinations, the proportion of severe imbalance exhibited a continuous decline, while moderate imbalance, basic coordination, moderate coordination and high-level coordination all displayed upward trends.

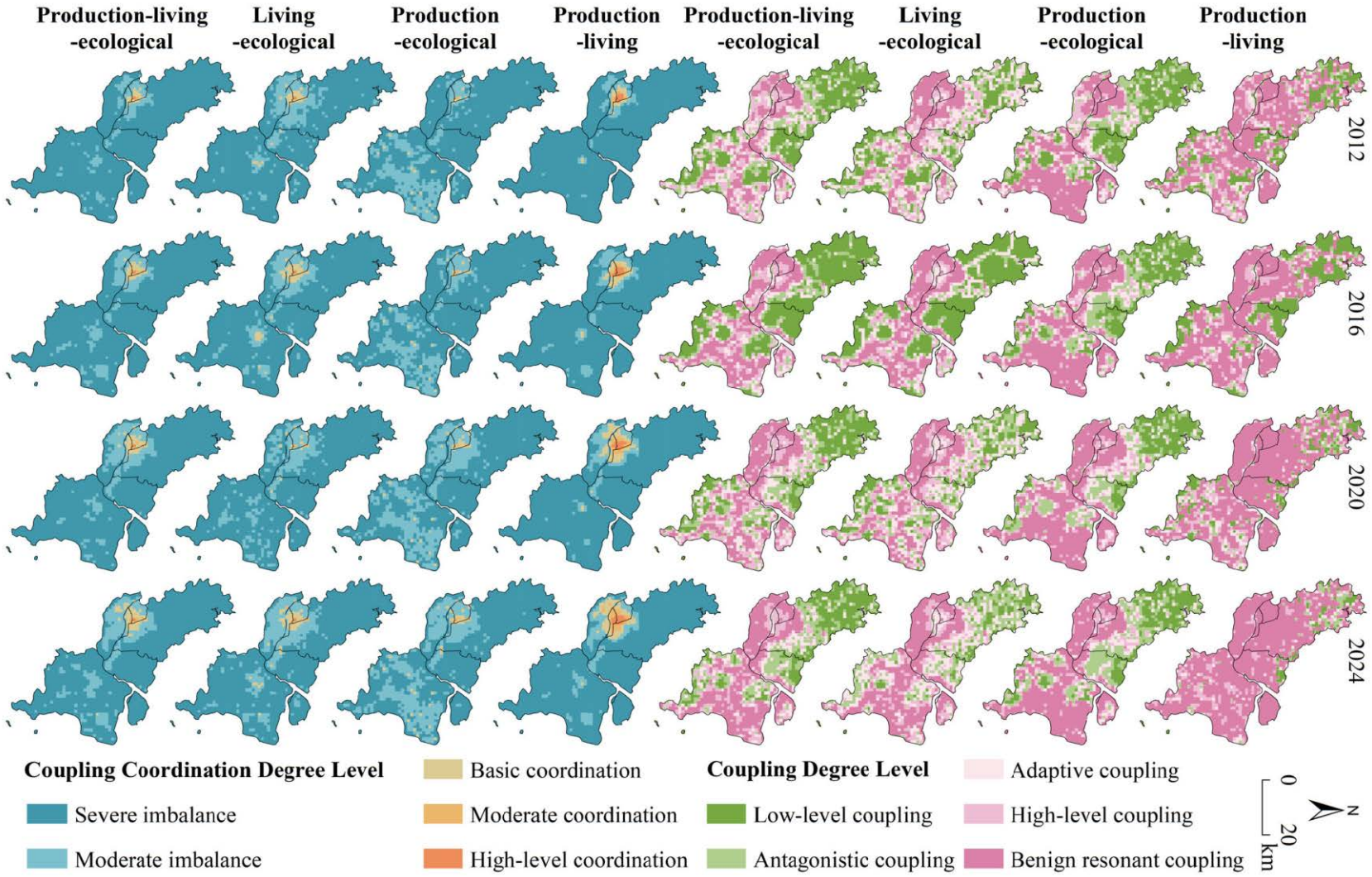


Figure 9. The spatiotemporal distribution of the coupling degree and coupling coordination degree of PLES functions from 2012 to 2024.

Overall, the PLES functions evolved toward greater degrees of coupling coordination. It is noteworthy that the coupling degree and coupling coordination degree among multifunctional systems are consistently greater in urban zones than in rural counterparts.

3.5. PLES Function Driving Factor Analysis

The GeoDetector factor detection results showed that all influencing factors, except aspect, had exerted significant effects on the comprehensive functions of PLES across the study area (Table 5). The *q*-statistic for aspect was zero throughout the study period, indicating that aspect barely affected regional PLES functions. During 2012–2024, GDP, population density, nighttime light intensity, slope and elevation exhibited an overall increase in explanatory power for PLES comprehensive functions, while distance to water bodies maintained a relatively stable and low *q* value. By contrast, socioeconomic factors (GDP, population density, and nighttime light intensity) yielded higher *q* values than natural geographic factors, indicating that they generally exerted stronger effects on the comprehensive functions of PLES.

Moreover, the explanatory capacity of pairwise factor interactions was universally higher than that of single independent factors, with most interactions exhibiting either nonlinear enhancement or two-factor enhancement patterns (Figure 10). Notably, interactions among socioeconomic factors, including GDP, population density, and nighttime light intensity, produced exceptionally high explanatory power for comprehensive functions of PLES. The interaction between GDP and population density maintained the highest *q* value throughout the study period, and its explanatory strength rose continuously over time. Interactions between socioeconomic factors and natural geographic factors also displayed growing explanatory capacity.

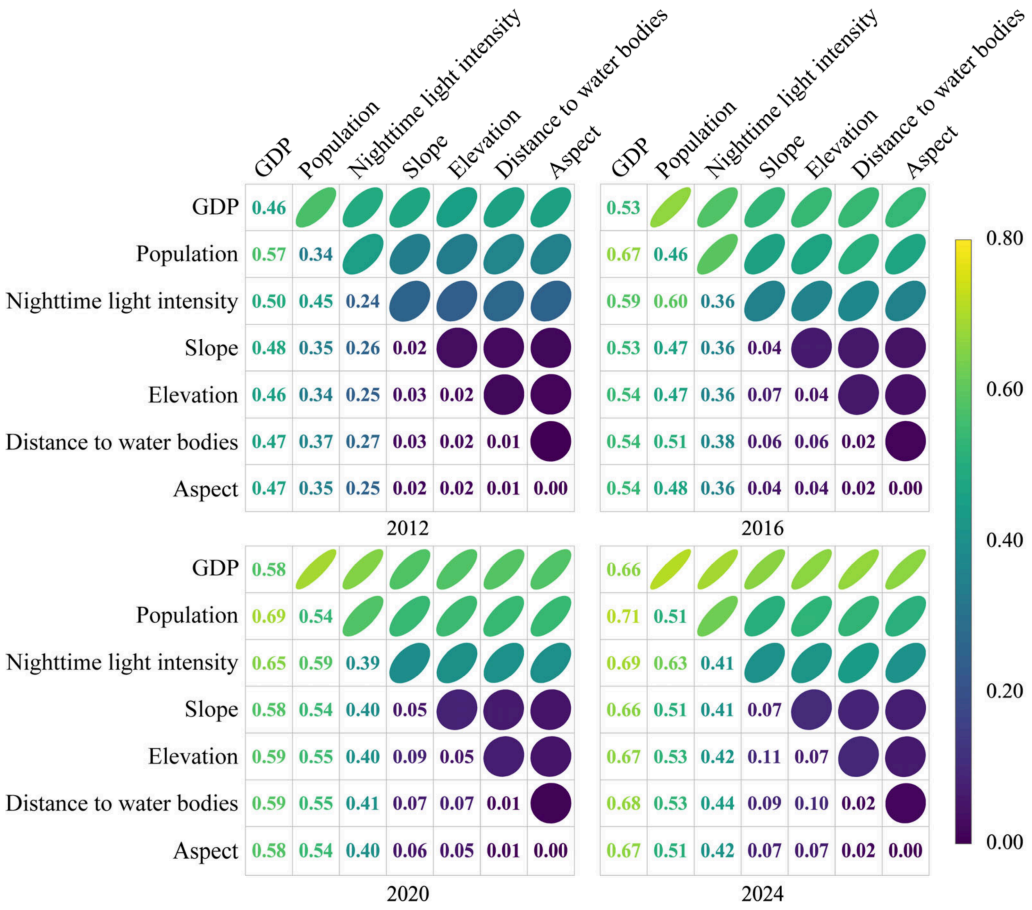


Figure 10. Interaction detection results of driving factors for comprehensive PLES functions.

Table 5. Deterministic value of driving variables from GeoDetector factor detection.

Year	GDP	Population Density	Nighttime Light Intensity	Slope	Elevation	Distance to Water Bodies	Aspect
2012	0.46 *	0.34 *	0.24 *	0.02 *	0.02 *	0.01 *	0.00
2016	0.53 *	0.46 *	0.36 *	0.04 *	0.04 *	0.02 *	0.00
2020	0.54 *	0.58 *	0.39 *	0.05 *	0.05 *	0.01 *	0.00
2024	0.51 *	0.66 *	0.41 *	0.07 *	0.07 *	0.02 *	0.00

* denotes significance at the $\alpha = 0.001$ level.

These results demonstrate that the comprehensive functions of PLES are jointly shaped by socioeconomic and natural geographical conditions, and paired driving factor interactions further strengthen their impacts on the comprehensive functions of PLES.

4. Discussion

4.1. Driving Mechanisms of Spatiotemporal Evolution of PLES Distribution and Functions

Natural geographical conditions constitute the basis shaping territorial spatial patterns and exert substantial influences on the spatiotemporal distribution and functional evolution of PLES [40]. GeoDetector results of the study reveal that the explanatory power of slope and elevation increased consistently from 2012 to 2024, indicating that topographic constraints have played a role in the evolution of PLES comprehensive functions to a certain degree. Our results indicate that midwestern and southeastern urban areas (i.e., Gulou, Taijiang, Cangshan and Changle) are predominantly composed of production- and living-dominated spaces (Figure 2). These regions are mostly covered by plains and gentle hills with low elevation and minimal topographic undulation, which offer favorable natural conditions for urban built-up land expansion and rational traffic network layout, further facilitating the advancement of production and living functions. Some rural zones in the mid-eastern part of the RUAFC (i.e., Jin'an and Mawei) with steeper slopes and higher terrain are constrained by topographic conditions and thus less vulnerable to urban expansion. Meanwhile, mountainous terrain is conducive to vegetation growth and ecosystem stability, resulting in these areas being predominantly preserved as ecologically dominated spaces [41]. This topography-constrained spatial differentiation is also consistent with existing observations from other rapidly urbanizing regions in China, where plains generally accommodate intensive production and living activities, while mountainous areas are dominated by ecological functions [42]. As illustrated in Figure 11, vegetated land is mainly distributed in northwestern rural mountainous areas (i.e., Jin'an and Mawei). In addition, the distribution of water systems also profoundly influences the territorial spatial pattern [43]. Waterfront areas, benefiting from abundant water resources and favorable living environments, are more prone to draw in population aggregation and urban construction [44], thereby affecting the distribution and evolution of PLES.

Compared with natural geographical conditions, socioeconomic factors exert stronger explanatory effects on PLES changes within the study area (Table 5). GeoDetector results indicate that population and GDP exert the most prominent influences on PLES evolution. As a rapidly urbanizing region in the Minjiang River Basin, the RUAFC's PLES distribution and functional evolution are closely associated with rapid socioeconomic development [45]. As shown in Figure 12, both GDP and population in the study area increased significantly from 2012 to 2024, with growth rates of 239.23% and 14.37%, respectively. Socioeconomic condition improvement promoted the continuous expansion of production- and living-dominated spaces, whose total area grew by 31.02 km^2 during 2012–2024. Meanwhile, economic growth continuously facilitated the improvement of public infrastructure and road conditions, enhancing urban livability and service accessibility [46]. These positive

conditions further stimulated population concentration and agglomeration in urban zones, thereby accelerating the restructuring of the territorial spatial pattern. This finding is also comparable to observations from other rapidly urbanizing metropolitan regions, where rapid economic growth and population agglomeration have been recognized as the primary drivers of PLES evolution and urban spatial restructuring [47].

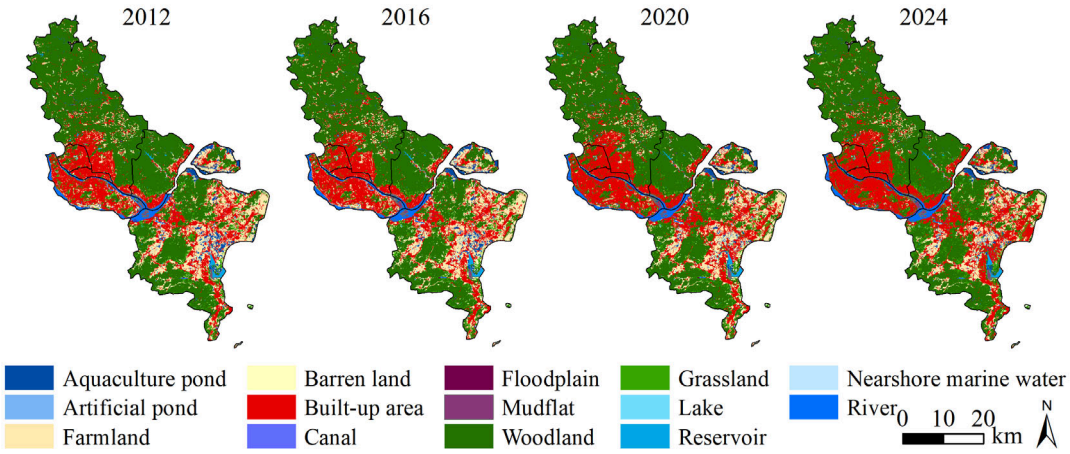


Figure 11. The spatiotemporal distribution of land cover in the study area during 2012–2024.

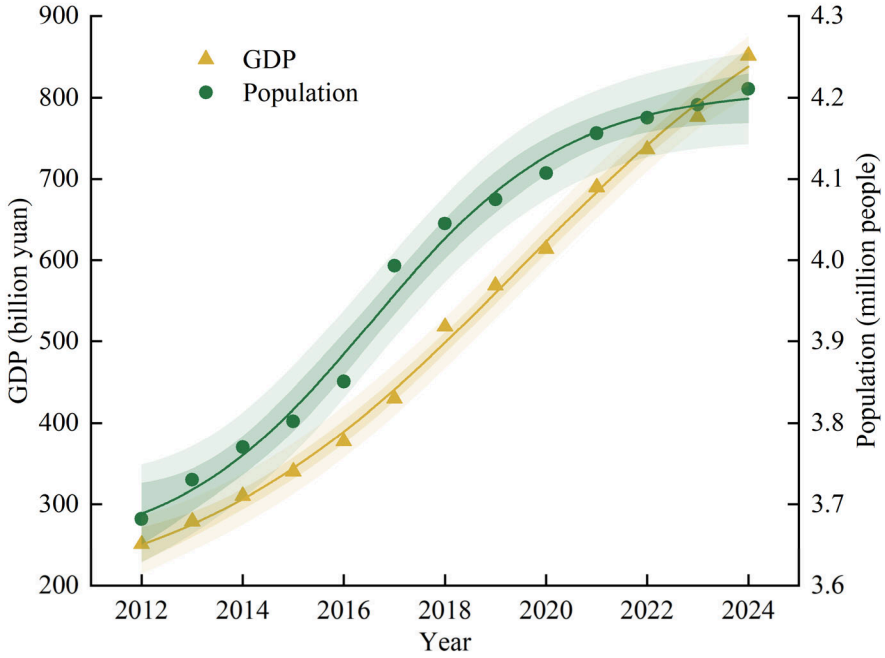


Figure 12. Change trend of GDP and population for the study area from 2012 to 2024.

Policies are another crucial human-driven factor affecting the spatiotemporal evolution of PLES [48]. Since the reform and opening-up, authorities have issued multiple regional development and territorial spatial plans, which seek to promote sustainable economic development by optimizing the spatial layout of territorial land. Various regional development policies and territorial spatial plannings have been successively formulated and implemented since 2012 (Figure 13). By delineating ecological conservation redlines, optimizing urbanization development boundaries, and guiding industrial layout and population agglomeration, these policies have facilitated the coordinated allocation and regulation of PLES at the macro level [49].

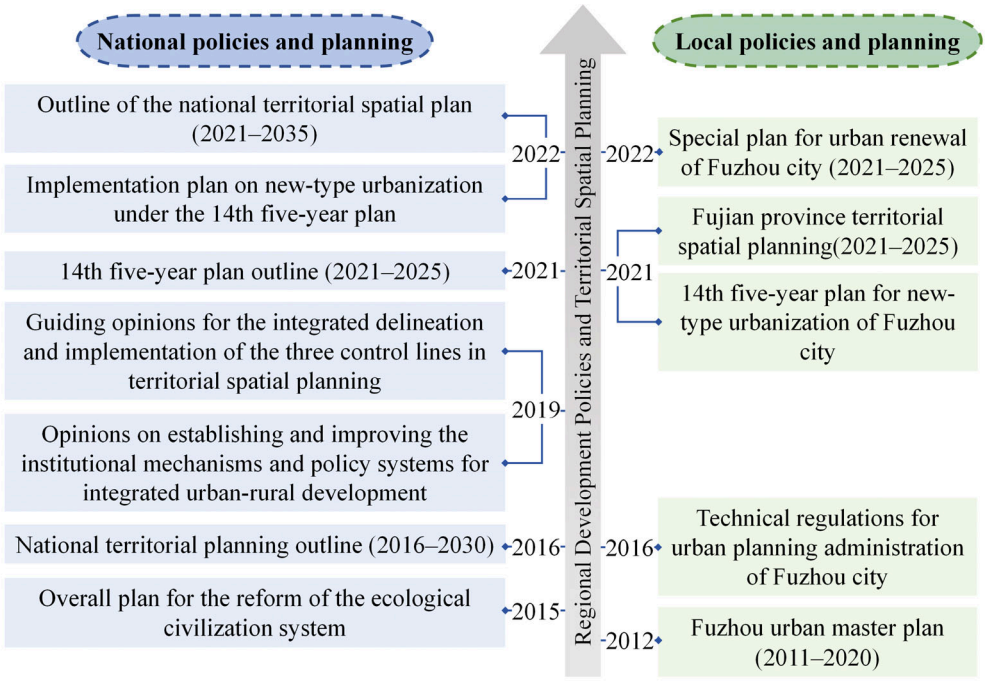


Figure 13. Development policies and territorial spatial planning of the study area during 2012–2024.

The spatiotemporal distribution and functional evolution of PLES are driven by various driving factors. According to the interaction detection results of the GeoDetector model, the explanatory intensity of pairwise driving factor is significantly stronger than that of individual factors, and all interaction types follow nonlinear enhancement and two-factor enhancement (Figure 9). Among all interaction combinations, socioeconomic factors show the strongest explanatory capacity. As Fuzhou's central urban region, the study area's PLES evolution is evidently driven by anthropogenic factors. Highly concentrated socioeconomic elements produce prominent synergistic superposition effects, which continuously promote structural restructuring and spatial evolution of PLES.

In summary, RUAFC's PLES evolution is jointly shaped by natural geographical conditions, socioeconomic development, and spatial planning policies. Interactions between socioeconomic drivers exhibit the most prominent explanatory effects, demonstrating that the spatiotemporal distribution and functional evolution of PLES within the study area are distinctly dominated by anthropogenic factors.

4.2. Methodological Advantages and Implications of the Study

As a complex and multifunctional composite system, territorial space exhibits obvious multi-scale characteristics and heterogeneous regularities in spatial patterns [50]. Depending solely on a single data source makes it difficult to accurately and finely depict the actual function of a spatial unit, especially in urban areas where functions are highly mixed [51]. Furthermore, fine-scale analysis can effectively distinguish differences in functional intensity across various PLES types, which helps uncover the spatial heterogeneity mechanism of territorial spatial functions and provides more reasonable scientific supports for territorial spatial planning and governance [52]. To achieve fine-scale PLES classification, this study constructs a hierarchical identification method based on a 3-ha hexagonal grid. It integrated remote sensing imagery and POI data, employed object-oriented random forest classification and the DBSCAN algorithm to delineate urban and rural boundaries, and further identified the PLES types based on established classification criteria. This framework fully considered the divergent distribution characteristics of PLES in urban and

rural areas, effectively overcoming the limitations of single data sources and substantially improving the precision and interpretability of the PLES identification outputs.

Against the backdrop of rapid urbanization, production, living and ecological functions interweave and interact dynamically. Evaluating only a single function fails to fully reflect the coordinated development of regional PLES systems [53]. The CCDM can effectively assess the interactive relationships and coordinated levels among multiple functional systems [54]. Accordingly, this research adopts the model to quantify coupling coordination degrees of binary PLES combinations and an integrated three-function system, thereby clarifying the level of coordinated development among different PLES functions and providing scientific evidence for identifying areas with function imbalance and optimizing territorial spatial layouts.

In conclusion, the methodological framework applied in the study offered an effective approach for fine-scale PLES identification and function coupling coordination evaluation. The findings contributed to territorial spatial optimization and provided practical implications for coordinated regional development.

4.3. Optimization Strategies for PLES Planning and Sustainable Territorial Development

Clarifying the spatiotemporal patterns and functional evolution characteristics of PLES is significant for optimizing land resource allocation and promoting territorial space development [55]. The findings of this study on spatiotemporal evolution, driving factor analysis, and coupling coordination degree evaluation of PLES can provide practical guidance for optimizing spatial structure, coordinating functional layouts, and advancing coordinated regional development.

First, public services and infrastructure facilities should be continuously upgraded to improve residents' well-being and living convenience. For production- and living-dominated urban areas with concentrated populations and high demands for living functions, priority should be given to boosting the efficiency of existing construction land through urban renewal, compact development and public service facility optimization, rather than pursuing excessive land expansion. For rural and peri-urban areas with relatively inadequate living support services, targeted investments in transportation, healthcare, education, and community services should be implemented to improve accessibility and better meet local development demands.

Second, strict compliance with ecological conservation redlines and the ecological security pattern is essential to prevent the encroachment of construction activities on core ecological spaces. For ecological-dominated mountainous areas identified in this study, ecological protection should remain the primary objective, while low-impact industries compatible with ecological conservation should be appropriately encouraged. Within the ecological carrying capacity, ecological leisure, cultural tourism, and health-oriented functions should be appropriately developed to maximize the service value of ecological spaces and balance ecological conservation and moderate development.

Third, the coordinated development of PLES functions should be promoted in an integrated manner, with particular emphasis on addressing functional shortcomings and enhancing the integration of the three functions. For regions with low coupling coordination levels or evident functional imbalance, targeted optimization measures should be implemented. Production-dominated areas should lessen over-reliance on resource-intensive development and facilitate industrial transformation and upgrading to alleviate conflicts between production expansion and ecological conservation. Areas lacking sufficient living functions need to improve public services and infrastructure to resolve mismatches between population layout and living carrying capacity. Ecologically advantaged areas

should foster low-impact industries, such as ecological tourism, to boost synergies between ecological value realization and socioeconomic development.

4.4. Limitations and Future Research Perspectives

PLES identification accuracy relies heavily on the quality of remote sensing data, and high-resolution spatial datasets can effectively improve classification performance [56]. This study extracted land use information using medium-resolution remote sensing imagery from the Landsat and Sentinel series, which inevitably restricted further improvements in the accuracy of PLES identification. Although fine-scale PLES classification was conducted at 3-ha hexagonal grid units in this study, subtle microscale functional disparities within individual grids may still be overlooked, especially in functionally mixed and highly urbanized areas. In addition, the spatial coverage, update frequencies, and collection standard of POI data vary across years. Although a series of preprocessing procedures have been implemented to mitigate analytical deviations, the inherent limitations of POI datasets still cannot be completely eliminated, which may introduce subtle deviations into urban-rural functional analysis. Moreover, urban and rural grids were delineated via the DBSCAN algorithm based on POI density. Although the classification results were further calibrated using township administrative boundaries and land use data, areas with sparse or missing POI records may still introduce uncertainties into urban-rural delineation. For example, some urban areas with limited POI records may be misidentified, while suburban market towns and industrial parks in rural peripheries with intensive human activities remain prone to misclassification as urban areas.

The building's three-dimensional structure exerts a notable impact on living function carrying capacity. High-rise residential buildings can generally undertake stronger living functions than low-rise ones with the same floor area [57]. Due to data accessibility constraints, building three-dimensional structure features were not integrated into the PLES function assessment system. Furthermore, the study primarily explored the spatiotemporal distribution patterns, driving factors, and coordinated development levels of PLES functions. It focused on depicting the current patterns and evolutionary processes of PLES, but did not simulate or predict future evolutionary trends.

To overcome such constraints, future studies could integrate higher-resolution remote sensing imagery and building structural data to conduct more refined PLES classification and functional evaluation, further improving the precision and accuracy of the results. Moreover, multi-scenario simulation and future prediction methods could be incorporated to analyze the PLES evolutionary trends under different development pathways, which can deepen the understanding of the dynamic territorial spatial evolution.

5. Conclusions

Clarifying the spatiotemporal distribution, functional characteristics, and coupling coordination status of PLES is critical for promoting spatial optimization and regional development. In this study, a comprehensive analytical framework was developed for fine-scale identification, function evaluation, coupling coordination assessment, and driving mechanism exploration of PLES by integrating multi-source remote sensing, POI, and socioeconomic data. By adopting a hierarchical identification method that combines object-oriented random forest classification with DBSCAN spatial clustering, the study effectively improved the accuracy of PLES classification using remote sensing imagery and POI data. Spatially, ecological-dominated spaces remained predominant, while living space expanded significantly, squeezing production and ecological spaces. In terms of functional changes, the overall PLES function exhibited an upward trend, with production function growing most rapidly, living function steadily improving, and ecological function maintaining

relative stability. The coupling coordination level of PLES functions continuously improved, though regional disparities remained evident, with highly coordinated areas concentrated in midwestern urban areas. The findings can serve as reliable references for territorial spatial planning and coordinated development in other similar rapidly urbanizing cities.

Supplementary Materials: The following supporting information can be downloaded at: https://www.mdpi.com/article/10.3390/rs18162721/s1, Table S1. Confusion matrices of land use classification for the study area in 2012, 2016, 2020, and 2024. Table S2. Number of verification sample points for each land use type in the study area. Figure S1. Spatial distribution of validation sample points in the study area for 2012, 2016, 2020, and 2024.

Author Contributions: Conceptualization, C.L.; methodology, C.L. and L.C.; software, L.C. and X.L.; validation, C.L. and L.C.; formal analysis, C.L., L.C. and X.L.; investigation, L.C. and X.L.; resources, Z.H.; data curation, Z.Y.; writing—original draft preparation, C.L., L.C. and X.L.; writing—review and editing, C.L.; visualization, C.L., L.C. and X.L.; supervision, C.L.; project administration, C.L.; funding acquisition, C.L. All authors have read and agreed to the published version of the manuscript.

Funding: This study was supported by the Social Science and Humanity on Young Fund of the Ministry of Education of China (No. 21YJCZH100), the Fujian Natural Science Foundation General Program (No. 2024J01414), and the Science and Technology Innovation Special Fund Project of Fujian Agriculture and Forestry University (No. KFB25039A, No. KFB24047).

Data Availability Statement: The remote sensing imagery used in this study was derived from Google Earth Engine (https://earthengine.google.com/, accessed on 26 June 2026). The NPP/VIIRS nighttime light imagery was obtained from the NOAA National Geophysical Data Center (https://www.ngdc.noaa.gov/eog/download.html, accessed on 26 June 2026). The digital elevation model (DEM) dataset was derived from Geospatial Data Cloud (https://www.gscloud.cn/, accessed on 26 June 2026). The point-of-interest (POI) dataset used in this study was acquired from the Amap API Platform (https://lbs.amap.com/api/webservice/, accessed on 26 June 2026). The road network dataset analyzed in this study was obtained from OpenStreetMap (https://www.openstreetmap.org/, accessed on 26 June 2026). The population size dataset was collected from LandScan (https://landscan.ornl.gov/, accessed on 26 June 2026). The datasets of annual average precipitation were provided by the National Tibetan Plateau Data Center (https://data.tpdc.ac.cn/home, accessed on 26 June 2026). The actual evapotranspiration dataset was acquired via the NASA Earthdata Data Portal (https://earthdata.nasa.gov/, accessed on 26 June 2026). The bedrock depth data came from the Global Depth to Bedrock Dataset (https://soilgrids.org/, accessed on 26 June 2026). Statistical data including GDP, primary industry output value and grain output were all retrieved from the official website of Fujian Provincial Bureau of Statistics (https://tjj.fujian.gov.cn/, accessed on 26 June 2026).

Conflicts of Interest: The authors declare no conflicts of interest.

References

1. Zhang, W.; Yuan, Q.; Cai, H. Unravelling Regional Development through the Production-Living-Ecological Perspective: Assessing Heterogeneity and Expert Insights. *Urban Clim.* **2024**, *55*, 101937. [CrossRef]
2. Li, C.; Wu, J. Land Use Transformation and Eco-Environmental Effects Based on Production-Living-Ecological Spatial Synergy: Evidence from Shaanxi Province, China. *Environ. Sci. Pollut. Res.* **2022**, *29*, 41492–41504. [CrossRef] [PubMed]
3. Lin, G.C.S.; Yi, F. Urbanization of Capital or Capitalization on Urban Land? Land Development and Local Public Finance in Urbanizing China. *Urban Geogr.* **2011**, *32*, 50–79. [CrossRef]
4. Lambin, E.F.; Meyfroidt, P. Global Land Use Change, Economic Globalization, and the Looming Land Scarcity. *Proc. Natl. Acad. Sci. USA* **2011**, *108*, 3465–3472. [CrossRef] [PubMed]
5. Raihan, A. Sustainable Human Settlements in the 21st Century: A Multidimensional Review of Challenges and Solutions. *Hum. Settl. Sustain.* **2026**, *2*, 83–107. [CrossRef]
6. Zhang, B.; Ren, Z.; Miao, Z.; Wang, L.; Wang, C.; Zhang, P.; Hong, S.; Wang, X.; Meng, F.; Huang, B. Strong Increase in Coverage but Accelerated Fragmentation in China's Urban Forests under Rapid Urbanization. *Appl. Geogr.* **2025**, *185*, 103793. [CrossRef]

7. Liu, M.; Wei, H.; Dong, X.; Wang, X.-C.; Zhao, B.; Zhang, Y. Integrating Land Use, Ecosystem Service, and Human Well-Being: A Systematic Review. *Sustainability* **2022**, *14*, 6926. [CrossRef]
8. Ni, M.; Zhao, Y.; Ma, C.; Jiang, W.; Xie, Y.; Hou, X. Spatial Identification and Change Analysis of Production-Living-Ecological Space Using Multi-Source Geospatial Data: A Case Study in Jiaodong Peninsula, China. *Land* **2023**, *12*, 1748. [CrossRef]
9. Wubuli, J.; Xue, D.; Song, Y.; Ma, B. Method for Identifying Rural PLES and Its Applications. *Ecol. Indic.* **2024**, *166*, 112273. [CrossRef]
10. Xiao, K.; Wang, N.; Liu, M.; Wang, Q.; Wang, J.; Ren, Y. Spatial Distribution and Influencing Factors of Cultural and Educational Facilities in Beijing: A POI-Based Analysis Using MGWR. *City Environ. Interact.* **2026**, *29*, 100312. [CrossRef]
11. Liu, L.; Tu, Y.; Sun, M.; Lyu, H.; Wang, P.; He, J. Spatial Quality Measurement and Characterization of Daily High-Frequency Pedestrian Streets in Xi'an City. *Land* **2024**, *13*, 885. [CrossRef]
12. Cao, Y.; Zhang, M.; Zhang, Z.; Liu, L.; Gao, Y.; Zhang, X.; Chen, H.; Kang, Z.; Liu, X.; Zhang, Y. The Impact of Land-Use Change on the Ecological Environment Quality from the Perspective of Production-Living-Ecological Space: A Case Study of the Northern Slope of Tianshan Mountains. *Ecol. Inform.* **2024**, *83*, 102795. [CrossRef]
13. Li, Y.; Zhao, J.; Zhang, S.; Zhang, G.; Zhou, L. Qualitative-Quantitative Identification and Functional Zoning Analysis of Production-Living-Ecological Space: A Case Study of Urban Agglomeration in Central Yunnan, China. *Environ. Monit. Assess.* **2023**, *195*, 1163. [CrossRef] [PubMed]
14. Song, W.; Cao, S.; Du, M.; He, Z. Aligning Territorial Spatial Planning with Sustainable Development Goals: A Comprehensive Analysis of Production, Living, and Ecological Spaces in China. *Ecol. Indic.* **2024**, *160*, 111816. [CrossRef]
15. Li, W.; Yi, P. Assessment of City Sustainability—Coupling Coordinated Development among Economy, Society and Environment. *J. Clean. Prod.* **2020**, *256*, 120453. [CrossRef]
16. Wang, L.; Wang, S.; Zhou, Y.; Liu, W.; Hou, Y.; Zhu, J.; Wang, F. Mapping Population Density in China between 1990 and 2010 Using Remote Sensing. *Remote Sens. Environ.* **2018**, *210*, 269–281. [CrossRef]
17. Dronova, I. Object-Based Image Analysis in Wetland Research: A Review. *Remote Sens.* **2015**, *7*, 6380–6413. [CrossRef]
18. Jia, M.; Liu, M.; Wang, Z.; Mao, D.; Ren, C.; Cui, H. Evaluating the Effectiveness of Conservation on Mangroves: A Remote Sensing-Based Comparison for Two Adjacent Protected Areas in Shenzhen and Hong Kong, China. *Remote Sens.* **2016**, *8*, 627. [CrossRef]
19. Lu, C.; Liu, J.; Jia, M.; Liu, M.; Man, W.; Fu, W.; Zhong, L.; Lin, X.; Su, Y.; Gao, Y. Dynamic Analysis of Mangrove Forests Based on an Optimal Segmentation Scale Model and Multi-Seasonal Images in Quanzhou Bay, China. *Remote Sens.* **2018**, *10*, 2020. [CrossRef]
20. Amini, S.; Saber, M.; Rabiei-Dastjerdi, H.; Homayouni, S. Urban Land Use and Land Cover Change Analysis Using Random Forest Classification of Landsat Time Series. *Remote Sens.* **2022**, *14*, 2654. [CrossRef]
21. Zhang, S.; Wei, H. Identification of Urban Agglomeration Spatial Range Based on Social and Remote-Sensing Data—For Evaluating Development Level of Urban Agglomeration. *ISPRS Int. J. Geo-Inf.* **2022**, *11*, 456. [CrossRef]
22. Jin, X.; Lu, Y.; Lin, J.; Qi, X.; Hu, G.; Li, X. Research on the Evolution of Spatiotemporal Patterns of Production-Living-Ecological Space in an Urban Agglomeration in the Fujian Delta Region, China. *Acta Ecol. Sin.* **2018**, *38*, 4286–4295. [CrossRef]
23. Liu, J.; Liu, Y.; Li, Y. Classification Evaluation and Spatial-Temporal Analysis of "Production-Living-Ecological" Spaces in China. *Acta Geogr. Sin.* **2017**, *72*, 1290–1304. [CrossRef]
24. Ji, Z.; Xu, Y.; Huang, A.; Lu, L.; Duan, Y. Spatial pattern and evolution characteristics of the production-living-ecological space in the mountainous area of northern Hebei Province: A case study of Zhangjiakou City. *Acta Sci. Nat. Univ. Pekin.* **2022**, *58*, 123–134. [CrossRef]
25. Tu, X.; Fu, C.; Huang, A.; Chen, H.; Ding, X. DBSCAN Spatial Clustering Analysis of Urban "Production–Living–Ecological" Space Based on POI Data: A Case Study of Central Urban Wuhan, China. *Int. J. Environ. Res. Public Health* **2022**, *19*, 5153. [CrossRef] [PubMed]
26. Zhang, S.; Fang, Y.; Zhao, X. POI Data–Driven Identification and Representation of Production–Living–Ecological Spaces at the Urban and Peri–Urban Scale: A Case Study of the Hohhot–Baotou–Ordos–Yulin Urban Agglomeration. *Sustainability* **2025**, *17*, 2235. [CrossRef]
27. Fu, C.; Tu, X.; Huang, A. Identification and Characterization of Production–Living–Ecological Space in a Central Urban Area Based on POI Data: A Case Study for Wuhan, China. *Sustainability* **2021**, *13*, 7691. [CrossRef]
28. Wang, W.; Zhao, Y.; Ma, C.; Dong, S. Identification and Analysis of Production–Living–Ecological Space Based on Multi-Source Geospatial Data: A Case Study of Xuzhou City. *Sustainability* **2025**, *17*, 886. [CrossRef]
29. Dou, Z.; Zhang, L.; Wang, S.; Xiao, S.; Zhao, Y. Identification of "Production-Living-Ecological" Space Based on Data Fusion: A Case Study of Tianjin City. *J. China Agric. Univ.* **2025**, *30*, 211–223.
30. Peng, Y.; Luan, Q.; Xiong, C. Evaluation of Spatial Functions and Scale Effects of "Production–Living–Ecological" Space in Hainan Island. *Land* **2023**, *12*, 1637. [CrossRef]

31. Yang, N.; Lu, C.; Ouyang, L.; Chen, R.; Man, W.; Wang, Z.; Lin, J.; Yu, Q.; Li, Z. Exploring Spatial–Temporal Evolution Patterns of Urban Heat Islands in Summer and Winter: Evidence from a Megacity of China. *Sci. Rep.* **2025**, *15*, 13592. [CrossRef] [PubMed]
32. Lei, X.; Liu, H.; Li, S.; Luo, Q.; Cheng, S.; Hu, G.; Wang, X.; Bai, W. Coupling Coordination Analysis of Urbanization and Ecological Environment in Chengdu-Chongqing Urban Agglomeration. *Ecol. Indic.* **2024**, *161*, 111969. [CrossRef]
33. Yang, Y.; Bao, W.; Liu, Y. Coupling Coordination Analysis of Rural Production-Living-Ecological Space in the Beijing-Tianjin-Hebei Region. *Ecol. Indic.* **2020**, *117*, 106512. [CrossRef]
34. Li, J.; Sun, W.; Li, M.; Meng, L. Coupling Coordination Degree of Production, Living and Ecological Spaces and Its Influencing Factors in the Yellow River Basin. *J. Clean. Prod.* **2021**, *298*, 126803. [CrossRef]
35. Dong, G.; Ge, Y.; Liu, J.; Kong, X.; Zhai, R. Evaluation of Coupling Relationship between Urbanization and Air Quality Based on Improved Coupling Coordination Degree Model in Shandong Province, China. *Ecol. Indic.* **2023**, *154*, 110578. [CrossRef]
36. Jiang, L.; Wu, Y.; He, X.; Fu, Q.; Wang, Z.; Jiang, Q. Dynamic Simulation and Coupling Coordination Evaluation of Water Footprint Sustainability System in Heilongjiang Province, China: A Combined System Dynamics and Coupled Coordination Degree Model. *J. Clean. Prod.* **2022**, *380*, 135044. [CrossRef]
37. Qiao, Y.; Wang, X.; Han, Z.; Tian, M.; Wang, Q.; Wu, H.; Liu, F. Geodetector Based Identification of Influencing Factors on Spatial Distribution Patterns of Heavy Metals in Soil: A Case in the Upper Reaches of the Yangtze River, China. *Appl. Geochem.* **2022**, *146*, 105459. [CrossRef]
38. Guo, Y.; Cheng, L.; Ding, A.; Yuan, Y.; Li, Z.; Hou, Y.; Ren, L.; Zhang, S. Geodetector Model-Based Quantitative Analysis of Vegetation Change Characteristics and Driving Forces: A Case Study in the Yongding River Basin in China. *Int. J. Appl. Earth Obs. Geoinf.* **2024**, *132*, 104027. [CrossRef]
39. Wang, J.; Xu, C. Geodetector: Principle and Prospective. *Acta Geogr. Sin.* **2017**, *72*, 116–134. [CrossRef]
40. Cui, X.; Xu, N.; Chen, W.; Wang, G.; Liang, J.; Pan, S.; Duan, B. Spatio-Temporal Variation and Influencing Factors of the Coupling Coordination Degree of Production-Living-Ecological Space in China. *Int. J. Environ. Res. Public Health* **2022**, *19*, 10370. [CrossRef] [PubMed]
41. Ji, Z.; Liu, C.; Xu, Y.; Sun, M.; Wei, H.; Sun, D.; Li, Y.; Zhang, P.; Sun, Q. Quantitative Identification and the Evolution Characteristics of Production—Living—Ecological Space in the Mountainous Area: From the Perspective of Multifunctional Land. *J. Geogr. Sci.* **2023**, *33*, 779–800. [CrossRef]
42. Wei, Y.; Zhou, P.; Zhang, L.; Zhang, Y. Spatio-Temporal Evolution Analysis of Land Use Change and Landscape Ecological Risks in Rapidly Urbanizing Areas Based on Multi-Situation Simulation—A Case Study of Chengdu Plain. *Ecol. Indic.* **2024**, *166*, 112245. [CrossRef]
43. Wang, S.; Yang, K.; Yuan, D.; Yu, K.; Su, Y. Temporal-Spatial Changes about the Landscape Pattern of Water System and Their Relationship with Food and Energy in a Mega City in China. *Ecol. Model.* **2019**, *401*, 75–84. [CrossRef]
44. Permana, A.S.; Astuti, W.; Er, E. Waterfront Development Concepts in Indonesia from the Perspective of Urban Planning and Environmental Sustainability. *Int. J. Built Environ. Sustain.* **2017**, *4*, 146–155. [CrossRef]
45. Bao, T.; Wang, R.; Song, L.; Liu, X.; Zhong, S.; Liu, J.; Yu, K.; Wang, F. Spatio-Temporal Multi-Scale Analysis of Landscape Ecological Risk in Minjiang River Basin Based on Adaptive Cycle. *Remote Sens.* **2022**, *14*, 5540. [CrossRef]
46. Yi, X.; Jue, W.; Huan, H. Does Economic Development Bring More Livability? Evidence from Jiangsu Province, China. *J. Clean. Prod.* **2021**, *293*, 126187. [CrossRef]
47. Cao, Y.; Huang, X.; Liu, X.; Cao, B. Spatio-Temporal Evolution Characteristics, Development Patterns, and Ecological Effects of "Production-Living-Ecological Space" at the City Level in China. *Sustainability* **2023**, *15*, 1672. [CrossRef]
48. Liu, H.; Zhang, M.; Feng, L.; Yun, S.; Zhang, F.; Yang, C. Driving Mechanisms and Adaptive Governance for Cultivated Land in Agro-Pastoral Ecotones: A 40-Year Empirical Study of Yulin City, China. *Remote Sens.* **2026**, *18*, 833. [CrossRef]
49. Gao, C.; Li, S.; Bao, H.; Zhang, Y. Multi-Dimensional Driving Mechanisms and Scenario Simulation of Production-Living-Ecological Space Evolution in Urban Agglomerations of China: Evidence from the Guanzhong Plain. *Land* **2025**, *14*, 2201. [CrossRef]
50. Hong, W.; Yang, S.; Guo, R.; Li, Y.; Jiang, L.; Li, X. Suitable Scale Structures for Urban Multi-Functions: An Integrative Approach Grounded in Socio-Ecological System Analysis. *Ecol. Process.* **2025**, *14*, 19. [CrossRef]
51. Zhang, Y.; Li, Q.; Tu, W.; Mai, K.; Yao, Y.; Chen, Y. Functional Urban Land Use Recognition Integrating Multi-Source Geospatial Data and Cross-Correlations. *Comput. Environ. Urban Syst.* **2019**, *78*, 101374. [CrossRef]
52. Chen, F.; Liu, Y. An Integrated Analysis Framework for Territorial Space Governance: Combining Land Use Classification and Functional Evaluation toward Spatial Zoning. *Habitat Int.* **2025**, *166*, 103572. [CrossRef]
53. Zhang, L.; Ji, X.; Su, Y.; Lu, Z. Spatial–Temporal Evolution and Coupling and Coordination of "Production–Life–Ecological" in Energy-Rich Area: A Perspective on Structure and Function. *Land* **2025**, *14*, 520. [CrossRef]
54. Dong, Q.; Zhong, K.; Liao, Y.; Xiong, R.; Wang, F.; Pang, M. Coupling Coordination Degree of Environment, Energy, and Economic Growth in Resource-Based Provinces of China. *Resour. Policy* **2023**, *81*, 103308. [CrossRef]

55. Xu, N.; Chen, W.; Pan, S.; Liang, J.; Bian, J. Evolution Characteristics and Formation Mechanism of Production-Living-Ecological Space in China: Perspective of Main Function Zones. *Int. J. Environ. Res. Public Health* **2022**, *19*, 9910. [CrossRef] [PubMed]
56. Yang, Y.; Huang, Q.; Wu, W.; Luo, J.; Gao, L.; Dong, W.; Wu, T.; Hu, X. Geo-Parcel Based Crop Identification by Integrating High Spatial-Temporal Resolution Imagery from Multi-Source Satellite Data. *Remote Sens.* **2017**, *9*, 1298. [CrossRef]
57. Wang, M.; Jia, Z.; Xiang, C. Multi-Objective Optimization Design of High-Rise High-Density Urban Morphology and Their Multidimensional Assessment of PV Capacity. *Sustain. Cities Soc.* **2025**, *130*, 106601. [CrossRef]

Disclaimer/Publisher's Note: The statements, opinions and data contained in all publications are solely those of the individual author(s) and contributor(s) and not of MDPI and/or the editor(s). MDPI and/or the editor(s) disclaim responsibility for any injury to people or property resulting from any ideas, methods, instructions or products referred to in the content.